Katja Elisabeth Goetschl, BSc

Effect of sulfate on Mg partitioning during its incorporation in calcite and on $CaCO_3$ polymorphism

MASTER'S THESIS

to achieve the university degree of

Master of Science

Master's degree programme: Earth Sciences

submitted to

Graz University of Technology

Supervisor

Univ.-Prof. Dr. rer. nat. Martin Dietzel

Dr. rer. nat. Vasileios Mavromatis

Graz, 09/2017

AFFIDAVIT

I declare that I have authored this thesis independently, that I have not used other than the declared sources/resources, and that I have explicitly indicated all material, which has been quoted either literally or by content from the sources used. The text document uploaded to TUGRAZonline is identical to the present master's thesis.

_____ _____

Date Katja E. Goetschl

Acknowledgements

I would like to express my special thanks and appreciation to my supervisor Βασίλης Μαυρομάτης for the great support, useful comments and his engagement through the learning process in the lab. Furthermore I would like to thank my supervisor Martin Dietzel for the valuable discussions, essential remarks and his support throughout and besides this master thesis. I would also like to thank Bettina Purgstaller for the helpful and enlightening discussions. Special thanks to Florian Konrad, Andre Baldermann, Judith Jernej and Patrick Grunert for their assistance with XRD, ICP-OES, IC and SEM analyses. Furthermore, thanks to Dorothee Hippler, Maria Hierz, Andrea Wolf and all the other colleagues from NAWI Graz Central Lab for Water, Minerals and Rocks for their great support in the lab. Without my friends and study colleagues, the time during my study would not have been the same. Thanks to Anna, Bea, Carina, Diana, Edith, Isa, Jana, Leni, Lukas, Mathias, Sabrina, Timo, Tom and Vera. Finally, I would like to express my deepest gratitude to my family. All that I am today is because of their love and support through the years.

Abstract

Chemical and isotopic signatures of trace elements/impurities in carbonate minerals are readily used in order to reconstruct environmental conditions occurring at the time of mineral formation. Previous experimental work has shown that the dominating parameters controlling Mg partitioning during calcite growth are temperature and growth rate. More recently the role of aqueous and/or surface metal-ligand complex formation has been recognized as an additional parameter affecting growth kinetics and elemental partitioning. In oceanic water, however, Ca and Mg form strong aquo-complexes with dissolved sulfate which may affect carbonate mineral formation in marine settings. This work aims to shed light on the effect of sulfate complexation with aqueous Ca^{2+} and Mg^{2+} ions during carbonate mineral growth. In order to evaluate the control of sulfate on Mg partitioning during its incorporation in calcite, chemical steady-state co-precipitation experiments on calcite seed material at 25 °C were performed. Throughout the experimental runs the aqueous Mg concentration was kept constant, whereas distinct growth rates ($10^{-8.0} \leq r_P \leq 10^{-6.9}$ mol m^{-2} s^{-1}) and different concentrations of dissolved SO_4^{2-} ($0 \leq SO_4 \leq 30$ mM) have been used. The results shown here indicate that the presence of dissolved sulfate has a strong impact on the incorporation of Mg in calcite and on the mineralogy of the precipitates. The precipitates collected after the experimental run consisted of either calcite or a mixture of calcite and aragonite dependent on SO_4 concentrations in the reactive solution and on growth rate. The Mg partitioning coefficient between calcite and reactive solution (D_{Mg} = $(Mg/Ca)_{calcite}$ / $(Mg^{2+}/Ca^{2+})_{(aq)}$) is higher at elevated calcite growth rate. In the absence of growth rate effects, the formation of sulfate-bearing complexes is suggested to control Mg uptake during calcite growth, where higher concentrations of dissolved sulfate in the reactive fluid resulted in significantly lower D_{Mg} values in calcite. The effect of sulfate on Mg partitioning can be described by two general mechanisms: First, the inhibition of calcite growth by aquo-complex formation between Ca^{2+} and SO_4^{2-} and second, the blocking of active growth steps by adsorption of foreign molecules, in this case sulfate-bearing complexes. Accordingly, adsorption of sulfate on crystal growth sites results in lower D_{Mg} values for calcite, likely due to competitive adsorption of Mg^{2+} and sulfate-bearing surface complexes. These results improve the general understanding of the controls of magnesium and sulfate on the formation of $CaCO_3$ minerals and its application to natural and applied systems.

Kurzfassung

Die Element- und Isotopensignaturen von inkorporierten Spurenelementen bzw. Verunreinigungen in Karbonatmineralen (z.B. Kalzit) werden häufig verwendet, um Umgebungsbedingungen zum Zeitpunkt der Mineralbildung zu rekonstruieren. Bisherige experimentelle Studien konnten zeigen, dass wesentliche Parameter, die z.B. den Mg-Einbau während des Kalzitwachstums kontrollieren, Temperatur und Wachstumsrate sind. Erst neuerdings wurde der Einfluss von gelösten Ionen bzw. von oberflächenassoziierten Metall-Liganden-Komplexen auf die Wachstumskinetik und den Einbau von Spurenelementen erkannt. Im Meerwasser bilden Ca- und Mg-Ionen sogenannte Aquakomplexe, assoziiert mit gelöstem Sulfat. Diese können in weiterer Folge Karbonatmineralbildung in mariner Umgebung beeinflussen. Die vorliegende Studie untersucht daher die Auswirkungen der Komplexbildung von Ca^{2+}- und Mg^{2+}-Ionen mit Sulfat-Ionen während des Karbonatmineralwachstums. Um den Effekt von Sulfat auf die Mg-Verteilung während der Inkorporation in Kalzit zu beurteilen, wurden Präzipitationsexperimente bei konstanten physikochemischen Bedingungen an vorgegebenen Kalzit Keimkristallen durchgeführt. Im Verlauf der Experimente wurde die Mg-Konzentration in der Lösung konstant gehalten, während unterschiedliche Wachstumsraten ($10^{-8,0} \leq r_P \leq 10^{-6,9}$ mol m^{-2} s^{-1}) und unterschiedliche Sulfat-Konzentrationen ($0 \leq SO_4 \leq 30$ mM) eingestellt wurden. Die Ergebnisse dieser Studie zeigen, dass die Anwesenheit von gelöstem Sulfat einen starken Einfluss auf den Einbau von Mg in Kalzit und auf die Mineralogie der Präzipitate hat. Die mineralogische Zusammensetzung der Präzipitate ergab entweder Kalzit oder eine Mischung aus Kalzit und Aragonit, abhängig von der SO_4-Konzentration in der Reaktionslösung und der Wachstumsrate. Der Mg-Verteilungskoeffizient zwischen Kalzit und Lösung ($D_{Mg} = (Mg / Ca)_{Kalzit} / (Mg^{2+} / Ca^{2+})_{(aq)}$) ist größer bei höheren Wachstumsraten von Kalzit. In Abwesenheit von Wachstumsrateneffekten beeinflusst die Bildung von sulfatgebundenen Komplexen den Mg-Einbau während des Kalzitwachstums, wobei höhere Konzentrationen an gelöstem Sulfat in der Reaktionslösung zu signifikant niedrigeren D_{Mg}-Werten in Kalzit führten. Der Effekt von gelöstem Sulfat in der Reaktionslösung auf den Mg-Einbau in Kalzit kann durch zwei allgemeine Mechanismen beschrieben werden: Erstens, die Hemmung des Kalzitwachstums durch Aquakomplexbildung zwischen Ca^{2+} und SO_4^{2-} und zweitens, die Blockierung von aktiven Wachstumspositionen an der Oberfläche von Kalzit durch Adsorption von Fremdmolekülen, in diesem Fall sulfatgebundenen Oberflächenkomplexen. Somit führt die Adsorption von Sulfat an Kristallwachstumspositionen wahrscheinlich aufgrund der kompetitiven Bildung von Mg^{2+}- und SO_4^{2-}-Oberflächenkomplexen zu niedrigeren D_{Mg}-Werten von Kalzit. Die Ergebnisse dieser Studie tragen zu einem besseren allgemeinen Verständnis der Auswirkungen von Magnesium und Sulfat bei der Bildung von Karbonatmineralen und deren Anwendungen in natürlichen und angewandten Systemen bei.

Content

1. Introduction

Calcium carbonate minerals ($CaCO_3$) are widely distributed in natural environments and have been extensively studied for their chemical, structural and isotopic composition (e.g. Morse and Mackenzie, 1990; Tucker and Wright, 1990; Weiner and Dove, 2003; Schlager, 2005; Dietzel, 2011). The two most common polymorphs of calcium carbonate in marine and meteoric depositional environments are calcite and aragonite. The occurrence and formation of carbonate minerals is in most cases related to precipitation from aqueous solutions where mineral growth proceeds along abiotic and biogenic pathways. Abiotic precipitation occurs via supersaturated solutions to form e.g. evaporites, ooids, lake deposits, etc. or it can also be induced by microbial activity. Bio-induced formation can occur due to increased supersaturation in respect to calcium carbonate as a by-product of common microbial metabolic activities like e.g. photosynthesis (Dupraz et al., 2004), ammonification (Rodriguez-Navarro et al., 2003), methane oxidation (Reeburgh, 2007), sulfate reduction (Braissant et al., 2007), etc.. Biogenic carbonate minerals are mostly related to skeletal material of calcifying organisms such as corals, bivalves, foraminifera or coccolithophores.

Elemental ratios (e.g. Mg/Ca, Sr/Ca and Ba/Ca) and isotopic compositions (e.g. $\delta^{18}/^{16}O$, $\delta^{44}/^{40}Ca$ and $\delta^{26}/^{24}Mg$) are widely used to reconstruct physicochemical conditions occurred during the formation of carbonates in depositional environments. The uptake of trace elements or impurities can be caused by isomorphic substitution of a host ion by foreign ions in a given crystal structure (McIntire, 1963). Note that the ideal divalent cation substitution is not the only case for foreign element incorporation into $CaCO_3$ although for instance trivalent REE (Voigt et al., 2017) and monovalent cations, e.g. Na^+ and Li^+ (Busenberg and Plummer, 1985; Marriott et al., 2004), are also present in natural occurring carbonates. In analogy the incorporation of anions in carbonates with the most well explored substitution to be that of boron in calcite and aragonite, owing to its dependence on pH (Mavromatis et al., 2015). The distribution behaviour of traces and impurities during mineral formation may depend on many different parameters such as crystal structure, temperature, pH, precipitation rate, solution chemistry, etc.. To understand, however, the parameters controlling the chemical composition of carbonate minerals, there is a vast demand for experimental work. Experimental work simplifies the system under investigation and explores how the different parameters are influencing the uptake of traces and impurities into calcium carbonate minerals. The evaluation of the controls on trace element substitution in $CaCO_3$ minerals requires also geochemical modelling, in particular derived from experimental studies but also from empirical and thermodynamic relationships.

The replacement of Ca by Mg is very common in sedimentary calcites with Mg concentrations that could exceed 25 mol% (Mavromatis et al., 2012). A large body of studies has been devoted in the last decades to characterize the impact of different physical and chemical parameters on the incorporation of Mg in marine carbonates (Mucci and Morse, 1983; Oomori et al., 1987; Busenberg and Plummer, 1989; Burton and Walter, 1991; Morse et al., 1997; Lin and Singer, 2009; Mavromatis et al., 2013), as Mg is the major divalent cation of seawater. To the best of our knowledge only one study (Mucci et al., 1989) has focused on systematically studying the effect of dissolved sulfate on Mg partitioning during its incorporation in calcite although sulfate is the second most concentrated anion in seawater (~28 mM at a salinity of 35 g/kg). Mucci et al. (1989) observed the Mg distribution coefficient in calcite precipitated from sulfate-free seawater which was 34 % larger than precipitated from "normal" seawater. A few studies have addressed the role of sulfate in controlling $CaCO_3$ polymorphism (Fernández-Díaz et al., 2010; Bots et al., 2011; Han et al., 2017), its incorporation in calcium carbonate (Kitano et al., 1975; Busenberg and Plummer, 1985) or its effect on calcite growth (Reddy and Nancollas, 1976; Nielsen et al., 2016). To shed light on the mechanisms controlling the formation of calcium carbonate and the Mg incorporation in the presence of sulfate, steady-state precipitation experiments with calcite seed material at 25 °C were performed. The results shown here allow for a first critical evaluation on the effect of sulfate on the incorporation of Mg into the calcite crystal lattice and are improving the general understanding of the controls of solution chemistry and growth rate on the formation of $CaCO_3$ minerals.

2. Theoretical background

2.1 $CaCO_3$ occurrence

Calcium carbonate ($CaCO_3$) occurs in three different anhydrous polymorphs: calcite, aragonite and vaterite. Calcite is the thermodynamically most stable $CaCO_3$ polymorph under Earth's surface conditions and has a trigonal symmetry. There appear to be four most important crystal forms of calcite which are rhombohedral, scalenohedral, prismatic and tabular (Okrusch and Matthes, 2014). Calcite is one of the most common minerals in sedimentary carbonates (Dietzel, 2011). Aragonite is less stable at ambient conditions and has an orthorhombic symmetry. The most common crystals of aragonite occur with a needle-like or acicular shape. Also common is the formation of repeated twinning which results in pseudo-hexagonal forms (Okrusch and Matthes, 2014). Aragonite can be formed e.g. from seawater by abiotic or biogenetic processes and is thus common in recent marine sediments (Gaetani and Cohen, 2006). As aragonite is thermodynamically metastable under ambient conditions, it tends to alter to calcite by dissolution and recrystallization after deposition (Hover et al.,

2001). Beside calcite and aragonite, the third anhydrous $CaCO_3$ polymorph vaterite is rarely occurring in nature, but found e.g. as a precursor phase during the transformation from amorphous calcium carbonate to calcite via vaterite (Xiao et al., 2010). Carbonate minerals are generally not pure substances in natural systems. The incorporation of trace elements or impurities can be caused by isomorphic substitution of metal ions with similar ionic charge and radius (Böttcher and Dietzel, 2010). Metal ions which are substituting the Ca^{2+} ion in $CaCO_3$ of the *calcite type* are e.g. Fe^{2+}, Mg^{2+}, Mn^{2+}, Cd^{2+} and Zn^{2+} (small cations) whereas for the *aragonite type* the Ca^{2+} is substituted by e.g. Ba^{2+}, Sr^{2+} and Pb^{2+} (large cations) (Dietzel, 2011). When crystal phases grow and incorporate foreign ions in their structure, also the thermodynamic stability can be significantly influenced as it is in the case of Mg-calcite, depending on the mole fraction of $MgCO_3$ (Mucci and Morse, 1984). For example at 25 °C, Mg-calcite containing 10 mol% Mg ($K_{sp} = 10^{-8.0}$), is more soluble than calcite ($K_{sp} = 10^{-8.42}$) or aragonite ($K_{sp} = 10^{-8.22}$) (Stumm and Morgan, 1996). However, the general formation of calcite, aragonite and/or vaterite strongly depends on additives such as inorganic ions or organic ligands, reaction kinetics and temperature (Niedermayr et al., 2013).

2.2 Formation of $CaCO_3$ from aqueous solution

To form a solid phase of $CaCO_3$ from aqueous solution, it is necessary to reach a certain threshold value in respect to its saturation state (Koutsoukos and Kontoyannis, 1984). The saturation index can be expressed by the following equation:

$$SI = log \frac{(Ca^{2+})(CO_3^{2-})}{K_{sp}} \quad (1)$$

where $(Ca^{2+})\cdot(CO_3^{2-})$ indicates the ion activity product (IAP) and K_{sp} stands for the solubility product of $CaCO_{3\,(s)}$. Supersaturation means that the aqueous ion activity product of the calcium and carbonate ion exceeds the K_{sp} value for $CaCO_{3\,(s)}$ (SI > 0). In general, the ionic compounds of $CaCO_3$ are dissolved in aqueous solution, but as soon as the solution becomes supersaturated with respect to a given solid, precipitation of $CaCO_3$ may occur. The precipitation of $CaCO_3$ from a slightly alkaline solution follows the equation

$$Ca^{2+} + HCO_3^- + OH^- \rightarrow CaCO_3 + H_2O \quad (2)$$

and there exist two general pathways on how precipitation can proceed. The most common way is the precipitation via growth of seed crystals, where the surface of the seed crystal acts as a nucleation site. The second pathway is the spontaneous nucleation from a homogeneous supersaturated solution, where a free energy barrier must be exceeded (De Yoreo and Vekilov, 2003).

2.3 Ion activity and aqueous complexes

Ions in solution interact with each other and their effective concentrations are determined by the ion activity of the species *i* in the law of mass action:

$$(a_i) = \gamma_i \cdot [c_i] \tag{3}$$

The ion activity (a_i) is indicating how, for example, a Ca^{2+} ion would behave when there are no interactions with other ions in theoretically infinitively diluted solution (molar concentration c_i is equal to a_i) and is corrected for non-ideal behaviour by the activity coefficient γ_i considering electrostatic interaction with other dissolved ions. There are several models available to calculate the activity coefficient where each model has its own range of validity defined by the ionic strength of the solution. The ionic strength describes the number of electrical charges in the solution and is expressed by the equation

$$I = {}^1/_2 \sum c_i \cdot z_i^2 \tag{4}$$

where c_i is the molar concentration and z_i is the charge of the respective ion. $I < 0.1$ M is the limit for using the Debye-Hückel equation, whereas the Davis equation can be used for $I \leq 0.5$ M. In high-saline solutions ($I > 1$ M) the Pitzer equation provides a much more sophisticated ion interaction model.

The formation of aqueous complexes, like major cation complexes, e.g. $CaSO_4^0$, or metal complexes with organic ligands, occurs because dissolved compounds in aqueous solution may attach to each other due to electrostatic forces and chemical bonding. The formation of aqueous complexes can be described by equilibria of the type

$$Ca^{2+} + SO_4^{2-} \leftrightarrow CaSO_4^0 \tag{5}$$

and its distribution is obtained by the equation

$$K = \frac{(CaSO_4^0)}{(Ca^{2+})(SO_4^{2-})} \tag{6}$$

where K describes the stability constant of this ion-association reaction. The higher the K value, the more stable the complex is. Both, intensive aqueous complexing and low activity coefficients cause a decrease of the activity of “free” ions in an aqueous solution, thereby increasing the solubility of a given mineral which may influence also the incorporation behaviour and the mobility of trace metals (Appelo and Postma, 2005).

2.4 Adsorption

The adsorption of ions or molecules from aqueous solution on a solid surface takes place at the solid-solution interface. An empirical relationship which is describing the surface adsorption is called sorption isotherm. The sorption isotherm shows the relationship between the bulk aqueous concentration of an adsorbate and the amount adsorbed on surface sites at constant temperature and reflects equilibrium. The most simple sorption isotherm type is described by Freundlich:

$$\Gamma = K_{ad} \cdot c_i^n \tag{7}$$

where Γ is the sorbed concentration, c_i is the solute concentration and K_{ad} and n are empirical adsorption constant and reaction order, respectively. With the Freundlich equation, sorption extends infinitely with increasing concentrations, which is unrealistic since the number of sorption sites at the solid can be expected to be limited. The better theoretical background is therefore related to the Langmuir equation:

$$\Gamma = \frac{Q \cdot K_s \cdot c_i}{1 + K_s \cdot c_i} \tag{8}$$

where Q is the adsorption capacity of the surface and K_s stands for the partition coefficient which controls the extent of adsorption. The Langmuir isotherm limits the maximum mass adsorption through the parameter Q (Stumm and Morgan, 1996; Appelo and Postma, 2005).

The adsorption of reactive solutes at a given solid surface is part of a sequence of discrete reaction steps, which are controlling also the kinetics of carbonate mineral precipitation. The principles of crystal growth can thus be explained by atomic processes, where molecules and ions enter building positions on the crystal surface. Accordingly, carbonate precipitation in seawater is surface-controlled (Morse et al., 2007). Solute compounds enter e.g. solid kink sites either directly from solution or after adsorbing and diffusion across terraces (De Yoreo and Vekilov, 2003). Crystal growth can be also retarded due to the adsorption of foreign ions or molecules (Reddy and Wang, 1980). This so-called poisoning of the crystallization surface plays a fundamental role in calcite growth, both in nature and industrial application (Gratz and Hillner, 1993).

2.5 Ion partitioning coefficient between a solid carbonate and aqueous solution

The ion partitioning coefficient (D) between a solid carbonate and aqueous solution defines the isomorphic substitution of an element in a solid during its precipitation as a function of the composition of the aqueous solution (Böttcher and Dietzel, 2010). The D value describes the incorporation behaviour of a trace element vs. the main element in the solid and is related to respective activities in

the solid and in the aqueous solution (Glynn, 2000). D values may depend on the degree of disequilibrium conditions (Prieto, 2010), and on reaction kinetics and mechanisms of crystal growth (Putnis, 2010). The partitioning coefficient of a metal-ion (e.g. Me = Mg, Sr or Ba) into e.g. calcite can be expressed by the equation

$$D_{Me} = \frac{(Me/Ca)_{solid}}{(Me/Ca)_{fluid}} \quad (9)$$

where the composition of the solid-phase is described by its mole fraction and the composition of the fluid is given by the concentration of free aqueous ions. Divalent cations such as Mg^{2+}, Sr^{2+}, Ba^{2+}, Cd^{2+}, Mn^{2+} and Co^{2+} have been studied extensively during their incorporation in calcite and aragonite which depends on the growth rate (Lorens, 1981; Mucci and Morse, 1983; Tesoriero and Pankow, 1996; Terakado and Taniguchi, 2006; Tang et al., 2008; Mavromatis et al., 2013). The incorporation of a trace element vs. the main element (Ca^{2+}) in calcite or aragonite as a function of growth rate can be followed by Fig. 1. D_{Me} = 1 means, there is no preference between trace and main element during formation of a solid from a fluid phase. If D_{Me} > 1 it means an increased incorporation of the trace element against the main element – compared to the trace/main element ratio of the solution – can be observed (e.g. Sr incorporation in aragonite). For D_{Me} < 1, a decreased incorporation of the trace element against the main element can be observed (e.g. Mg incorporation in calcite). At high growth rates the system is controlled rather by kinetics than by thermodynamic equilibrium. During precipitation at high growth rates the Me^{2+}/Ca^{2+} ratio in the solid tends to get close to the respective ratio in the fluid, approaching D_{Me} = 1.

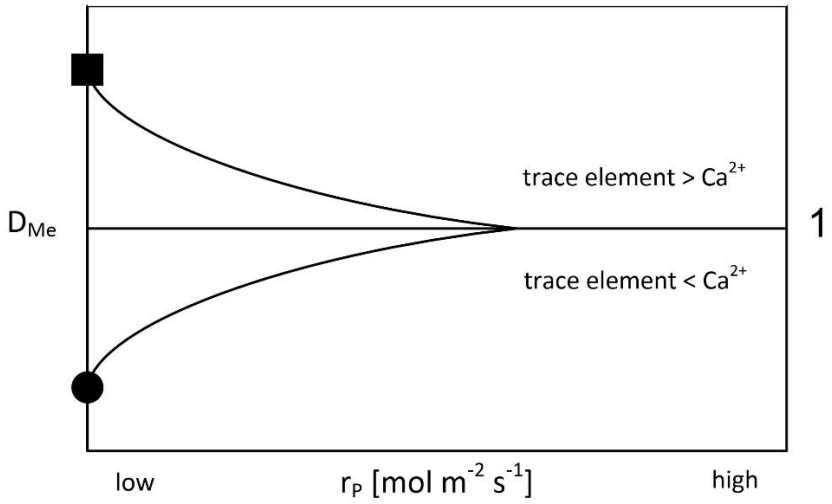

Fig. 1: Metal-ion partitioning coefficient (D_{Me}) as a function of growth rate (r_P). The incorporation of a trace element vs. the main element is strongly dependent on the precipitation/growth rate (r_P).

3. Methods

3.1 Experimental set-up

Low-Mg calcite precipitation experiments were carried out on synthetic pure calcite seeds at 25 °C and 1 bar pCO_2 using a mixed-flow reactor experimental set-up similar as previously described in Mavromatis et al. (2013; 2015; 2017). The experimental set-up used in the present study is illustrated in Fig. 2 and consists of two separate inlet solutions A and B, and a reaction vessel placed on a stirring plate in a constant temperature room. This design was adapted because it allows controlled physical-chemical conditions during the mineral growth. The inlet solution A contained $(Ca,Mg)Cl_2$, in which the Mg concentration was the same for every experiment and it was equal to the double of that present initially in the reactor in order to avoid its dilution by the addition of inlet solution B. The inlet solution B contained $Na_2(CO_3,SO_4)$, where the concentration of sulfate was also adjusted to the double of its concentration present in the initial reactor solution, which varied in the concentration range between 10 and 30 mM (see Table 1). The initial solution in the reactor of 0.5 L contained ~10 mM of $CaCl_2$ and $MgCl_2$ as well as different concentrations of Na_2SO_4 (Table 1). Note here that a single Mg source was used for all experiments by diluting a concentrated $MgCl_2$ stock solution in order to precisely constrain the Mg concentration and to ensure the uniform Mg isotope composition for future stable isotope measurements. Ionic strength of all solutions maintained constant during each experimental run and was set to 400 mM adjusted by the addition of NaCl if necessary.

To induce precipitation, both inlet solutions were pumped via a peristaltic pump in the reaction vessel at the equal flow rate of ~10 mL/day. The precipitation rate for $CaCO_3$ could be modified by changing the molalities of Ca^{2+} and CO_3^{2-} in the inlet solutions. During the whole experimental run the solution pH was kept constant at 6.3 ± 0.1 via continuous bubbling of CO_2 gas in the reaction vessel. The reactor solution was continously stirred at a constant rate of 300 rpm using a floating magnetic stir bar. All reacting solutions were prepared with analytical grade chemicals ($CaCl_2{\cdot}2H_2O$, $MgCl_2{\cdot}6H_2O$, Na_2CO_3, Na_2SO_4 and NaCl from Roth) dissolved in ultrapure deionized MQ water (Millipore Integral 3: 18.2 MΩ cm^{-1}). The initial amount of ~1 g synthetic calcite with a BET specific surface area of 0.29 m^2/g (see methods below) was used in all reactors as seed material to ensure the same conditions to the parameter of growth rate.

Every 24 hours a volume of the reactive fluid – equal to the total volume of the sum of the inlet solutions added in 24 hours (~20 mL) – was collected for chemical analyses with a syringe, so that the volume of the reactor solution maintained almost constant within ± 4 %. Prior to sampling the magnetic stirrers were stopped shortly to allow the solid material to settle down and to minimize its removal by sampling. In this way the solid/solution ratio was kept almost constant during the course

of an experiment. Directly after sampling, the collected solution was filtered through a 0.2 µm membrane cellulose acetate syringe filter and pH was measured with a calibrated pH electrode coupled to a meter (WTW Multi3420) using a 3-point calibration. An adequate amount of the sample was taken to measure the fluid carbonate alkalinity whereas the rest of the reactive fluid was acidified for further Ca, Mg, and S (SO_4) analyses. The duration of each experimental run was 12 days and at the end, the entire reactive solution was filtered through a 0.45 µm membrane using a vacuum filtration unit. The solid material was rinsed with MQ water and dried at 40 °C. In total, 20 experiments were performed and split in two sets with 10 experiments in each case. The first run of experiments was performed at varying growth rates but constant concentrations in respect to Mg (10 mM) and SO_4 (30 mM). In the second run, experiments were performed in duplicates, where the Mg concentration was kept constant, but the SO_4 concentration was adjusted to 10, 15, 20, 25 and 30 mM, respectively. One experiment of the duplicates was always conducted at low growth rate (log r_P = -7.6 ± 0.1 mol m^{-2} s^{-1}) and one conducted at high growth rate (log r_P = -7.0 ± 0.1 mol m^{-2} s^{-1}). Two experiments in the range of the lowest and highest growth rate were carried out without SO_4 (MgS9 and MgS10).

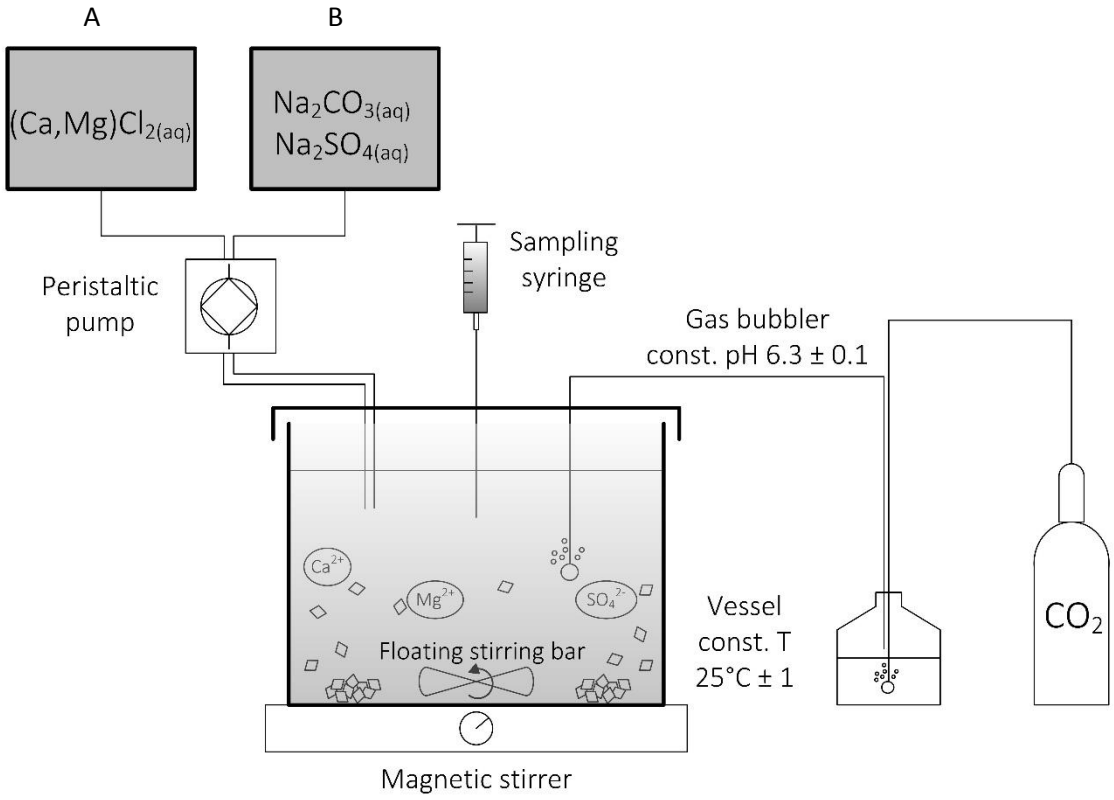

Fig. 2: Experimental set-up of the Mg co-precipitation experiments on calcite seed material in the presence and absence of sulfate under steady-state conditions. The mineral precipitation is induced by the simultaneous inflow of solutions A and B via a peristaltic pump at similar rates in the vessel. The pH is maintained constant at 6.3 ± 0.1 by continuous bubbling of CO_2 gas in the reactive solution.

3.2 Chemical and mineralogical analyses

3.2.1 Fluids

The chemical analyses of the collected solutions allowed recording the chemical evolution of the reactive fluids as a function of time. Ca, Mg and S (in this case referring to SO_4) concentrations were measured by Inductive Coupled Plasma Optical Emission Spectrometry (ICP-OES), using a PerkinElmer Optima ICP-OES 8300 DV with an analytical uncertainty of ± 3 %. The calibration ranges of concentrations for Ca 1-500 ppm, Mg 0.2-100 ppm and for S 10-100 ppm have been used and the samples were diluted accordingly. Note here that the reported concentrations assume that the measured concentration of S represents the concentration of SO_4 in the reactive solution. Due to the mineralogical analyses of experimental set 1, also the chemical evolution of Sr in the fluids of experimental set 2 was measured by ICP-OES. Sr was not explicitely added to the initial or inlet solutions, but as a trace impurity (< 0.01 %) of $MgCl_2$ and $CaCl_2$ which were used to prepare the reacting solutions. Measurements of pH were performed with a WTW SenTix®945 gel electrode, calibrated against NIST standard buffer solutions at pH 4.01, 7.00 and 10.00 with an uncertainty of ± 0.03 units. The total alkalinity of the fluids was determined by a Schott TitroLine alpha plus titrator using a 0.01 M HCl solution with an analytical precision of ± 2 %. The quantitative control of the measured S concentrations was performed by Ion Chromatography (IC) measurements. For this purpose, four selected experiments containing the lowest and highest concentration of SO_4 (MgS11, MgS12, MgS19 and MgS20) were measured, using a Dionex IC S 3000 with IonPac® AS19 and CS16 column, with an analytical precision of ± 3 %. These samples were diluted immediately after sampling without acidification and analysed S and SO_4 data were identical within ± 5 %.

The molalities of aqueous speciation in the reactive solutions, ion activities and saturation indices were calculated using the PHREEQC software in combination with its minteq.v4 database. The ion activity coefficients of free aqueous ions and charged complexes in this model are calculated by using the Davis equation. The reaction for precipitation of Mg-bearing calcite is defined according to the equation

$$(1-x)Ca^{2+} + xMg^{2+} + CO_3^{2-} \rightleftarrows Ca_{1-x}Mg_xCO_3 \quad (10)$$

Saturation state (Ω) with respect to calcite or aragonite is referred to the activities of the free ions and is expressed as:

$$\Omega_{CaCO_3} = \frac{(Ca^{2+})\,(CO_3^{2-})}{K_{sp}} \quad (11)$$

where K_{sp} = $10^{-8.48}$ for calcite and K_{sp} = $10^{-8.34}$ for aragonite at 25 °C respectively (Plummer and Busenberg, 1982). Note here that owing to the low presence of Mg in the synthetic precipitates of this

work, that does not exceed 1.7 mol% $MgCO_3$ as it can be seen in Table 1, the forming mineral has been considered to be calcite and no further modifications in Eq. 11 due to variations in solubility of Mg-rich calcite were considered similar to Mavromatis et al. (2013; 2017).

3.2.2 Solids

The specific surface area of the synthetic calcite seed material was determined by multi-point krypton adsorption using the Brunauer-Emmett-Teller (BET) method. Measurements were performed using a Quantachrome Autosorb-1 MP with an analytical uncertainty of ± 10 %. Powder X-ray diffraction (XRD) patterns of the solids collected at the end of the experimental run were recorded by a PANalytical X'Pert PRO diffractometer using Cu-Kα-radiation (40 mA, 40 kV) at a 2θ range from 15° to 60° and a scan speed of 0.03° s^{-1}. For qualitative characterization of crystalline products the PANalytical HighScore Plus software with the ICSD database was used and the mineral phases were quantified by Rietveld refinement. Analytical uncertainty of the quantification lies within 1 %. The precipitates were gold-coated and imaged using a ZEISS DSM 982 Gemini scanning electron microscope (SEM) equipped with a field emission gun operating at 2 kV accelerating voltage. Ca and Mg content of the solids were measured by ICP-OES after digestion in concentrated HNO_3. (10 M) and subsequent dilution with MQ water.

4. Results

4.1 Chemical evolution of the reactive solutions and growth rate calculation

Equilibrium concentration in terms of aqueous Ca concentration by using this experimental design was usually achieved within 4000 min, whereas a longer reaction time, between 8000 and 10000 min was necessary for the attainment of steady-state in terms of aqueous Mg concentration (Mavromatis et al., 2013). In this study, the chemical steady-state of Ca concentrations in the reactive solutions was achieved between 8000 and 11000 min depending on the concentrations in the inlet solutions (Fig. 3). Interestingly, in the two experiments conducted in the absence of sulfate (MgS9 and MgS10) and also in experiments MgS7, MgS8, MgS12, and MgS20, where the Ca concentrations of the inlet solution were higher compared to experiments conducted at lower growth rate, steady-state of Ca was attained about 3000 min earlier. Steady-state concentrations for Mg were reached within at least 8000 min of reaction time. Concentrations of SO_4 remained constant in the whole course of the experimental runs. The pH remained constant at 6.3 ± 0.1 for the duration of the whole experimental times. Carbonate alkalinity was increasing at the beginning of the experiments due to the continuous addition of the inlet solution B and achieved steady-state caused by precipitation of carbonate and the attainment of

chemical steady-state in the reactive solution. Note here that the results show a significant decrease of alkalinity (5-10 mM) and Ca (3-5 mM) on day six of the experimental course that can be explained by carbonate precipitation at a larger extent. This event can be correlated with a significant decrease of the Sr concentration in the reactor solution for those experiments which contained precipitated aragonite. In Fig. 4 it is clearly shown that there was an ongoing decrease of aqueous Sr from day 6 on in experiment MgS7. Aqueous Mg/Ca compositions of the inlet and the reactive solutions are reported in Table 1. The distribution of aqueous Ca and Mg species was calculated using PHREEQC and is shown in Table A in the Appendix.

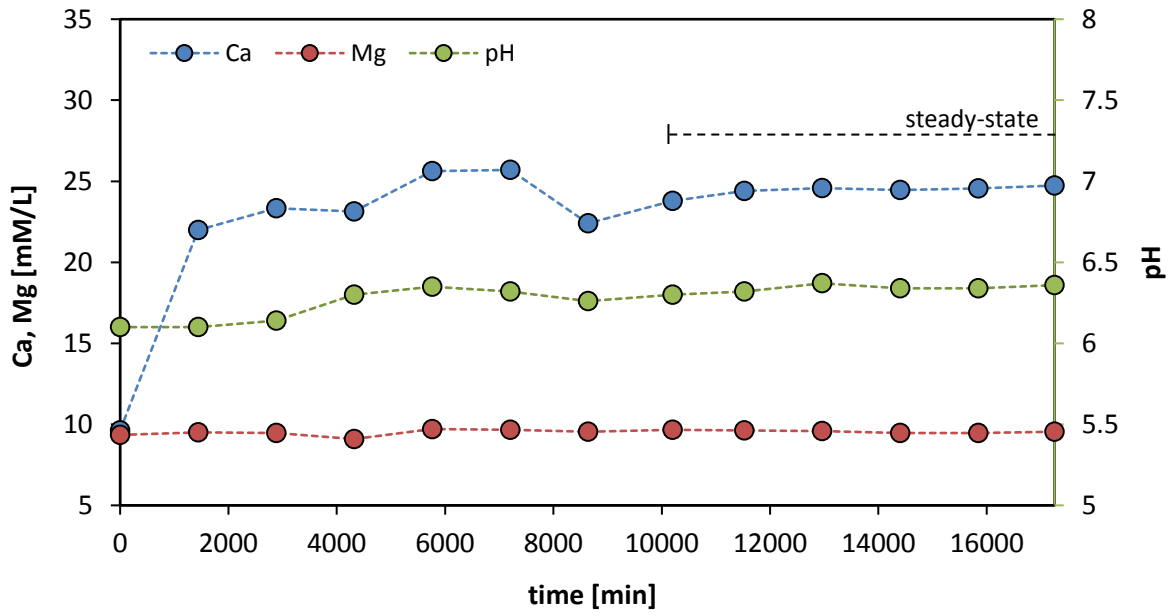

Fig. 3: Concentrations of Ca and Mg and evolution of pH value in the reactive solution as a function of time for experiment MgS15 performed in the presence of 20 mM sulfate. Chemical steady-state conditions were achieved after 10000 min which is indicated by the dotted line. Analytical uncertainty is included in symbol size.

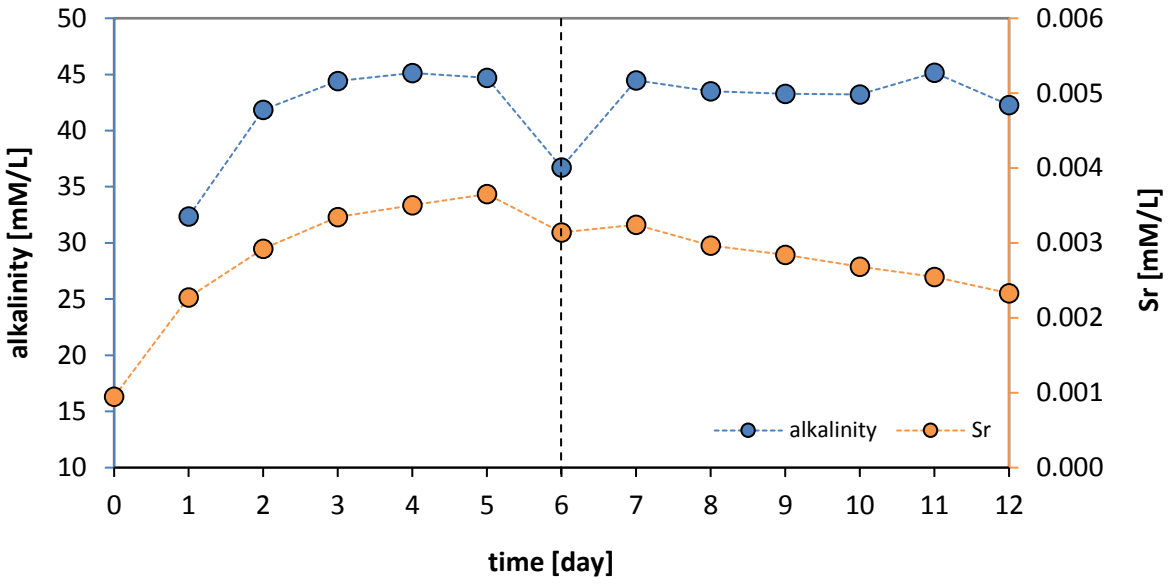

Fig. 4: Concentration of Sr and evolution of alkalinity over time for experiment MgS7. There was a prominent decrease of Sr concentration and alkalinity on day 6, which was noted in most of the experiments. Analytical uncertainty is included in symbol size.

The calculation of calcite growth rate r_P (mol m^{-2} s^{-1}) at steady-state conditions can be estimated by the moles of Ca and Mg added in the reactor in 24 hours, corrected for the moles of Ca and Mg removed from the reactor via sampling during the same period of time. Calcite growth rate was estimated as

$$r_p = \frac{n_{Ca(add)} + n_{Mg(add)} - n_{Ca(rem)} - n_{Mg(rem)}}{86400} / S \quad (12)$$

where $n_{Ca(add)}$ and $n_{Mg(add)}$ refer to the moles of Ca and Mg respectively added in the reactor within 24 hours and $n_{Ca(rem)}$ and $n_{Mg(rem)}$ denote the moles of Ca and Mg respectively removed from the reactor within 24 hours. The r_p value is calculated based on the average molar concentrations at steady-state conditions. The value 86400 in Eq. 12 represents the number of seconds per day and S stands for calcite total surface in m^2 which includes the surface of seed material and precipitated material estimated by the difference of added and removed steady-state aqueous concentrations of Ca and Mg in the reactive solutions. Calculated calcite growth rates (r_P) range from $10^{-8.0}$ to $10^{-6.9}$ mol m^{-2} s^{-1} with an estimated error of about ± 0.1 log units. For the precipitates, which contained aragonite beside calcite, it was not possible to correct the growth rate for the precipitated aragonite because it is not definite at which time point aragonite started to precipitate.

Table 1: Concentrations of inlet solutions and reactive solutions ($_{ss}$ stands for steady-state conditions), pH value, calculated precipitation rates, Mg content of final precipitate measured by chemical digestion and ICP-OES analyses, partitioning coefficients, saturation state with respect to calcite, mass of precipitate and proportions of calcite and aragonite.

	solution					solid						
Experiment	**Inlet solution**	**SO_4**	**Ca_{ss}**	**Mg_{ss}**	**pH_{ss}**	**Log r_P**	**X_{Mg}**	**Log D_{Mg}**	**$\Omega_{calcite}$**	**Precipitate[a]**	**Calcite**	**Aragonite**
	Mg/Ca	(× 10^{-3} M)	(× 10^{-3} M)	(× 10^{-3} M)		(mol m^{-2} s^{-1})	(mol%)			(g)	[wt. %]	[wt. %]
MgS1	0.40	30	15.38	7.39	6.35	-7.82	0.4	-2.15	1.8	0.49	100.0	-
MgS2	0.20	30	23.87	9.55	6.38	-7.56	0.7	-1.77	3.4	0.98	100.0	-
MgS3	0.20	30	23.76	7.93	6.37	-7.50	0.7	-1.73	3.4	1.06	100.0	-
MgS4	0.10	30	23.39	8.62	6.44	-7.18*	0.9	-1.64	4.4	2.48	94.6	5.4
MgS5	0.08	30	24.78	8.97	6.41	-7.08*	1.0	-1.60	4.2	3.25	90.1	9.9
MgS6	0.08	30	29.07	9.66	6.41	-7.08*	1.0	-1.56	5.0	3.21	87.6	12.4
MgS7	0.06	30	27.68	9.45	6.45	-6.98*	1.2	-1.49	5.4	4.50	41.3	58.7
MgS8	0.05	30	26.24	9.19	6.43	-6.92*	0.9	-1.62	4.5	5.34	61.5	38.5
MgS9	0.40	-	18.73	9.96	6.18	-7.99	0.8	-1.85	1.4	0.32	100.0	-
MgS10	0.05	-	22.82	8.77	6.20	-6.92	1.7	-1.38	1.9	5.46	100.0	-
MgS11	0.20	10	22.02	9.73	6.29	-7.68	0.9	-1.73	2.7	0.66	100.0	-
MgS12	0.06	10	25.74	9.35	6.39	-6.97	1.2	-1.50	4.8	4.39	100.0	-
MgS13	0.20	15	26.84	10.13	6.28	-7.63	0.6	-1.81	3.3	0.75	100.0	-
MgS14	0.06	15	24.80	8.95	6.45	-6.97	1.1	-1.54	5.6	4.45	100.0	-
MgS15	0.20	20	24.54	9.56	6.34	-7.57	0.7	-1.80	3.7	0.89	100.0	-
MgS16	0.06	20	34.58	9.66	6.43	-6.99*	0.8	-1.59	7.1	4.18	96.3	3.7
MgS17	0.20	25	25.56	9.86	6.32	-7.60	0.6	-1.82	3.3	0.81	100.0	-
MgS18	0.06	25	25.55	9.45	6.49	-7.05*	1.0	-1.60	6.8	3.47	90.2	9.8
MgS19	0.20	30	26.66	10.16	6.31	-7.74	0.6	-1.88	3.5	0.58	100.0	-
MgS20	0.06	30	32.05	9.91	6.48	-7.03*	0.9	-1.59	7.6	3.76	75.6	24.4
Seed							1.4E-02					

[a] Precipitated material per 12 days.

*Growth rate estimation is affected by the presence of aragonite in the final precipitate

4.2 Mineralogy and chemical composition of the precipitated phases

Quantitative XRD results suggest that the solid material collected after the experimental runs consist of calcite, except for 8 samples that consist of calcite and aragonite. The mineralogical compositions of the precipitates, as well as the proportion of the two mineral phases are reported in Table 1. The amount of precipitated aragonite ranges from 3.7 to 58.7 wt. % with larger percentages to be observed in experiments conducted at higher growth rates. Precipitation of aragonite was detected in experiments conducted at 20 mM, 25 mM and 30 mM sulfate concentration in the reactive solution, but only at elevated growth rates (see Fig. 5). In experiments (i) with low sulfate concentrations of 10 mM and 15 mM in the reactive solution at high growth rate and (ii) in experiments conducted at low growth rates and sulfate concentrations ranging from 10 to 30 mM, the precipitate was consisting of 100 wt. % calcite. The calcite pattern of all samples analyzed in this study do not exhibit differences compared to the calcite seed material and no shift of the characteristic $d_{(104)}$ calcite peak to lower d-values due to Mg incorporation in the crystal lattice was observed (corresponding to calcite containing $MgCO_3$; (Goldsmith et al., 1961)).

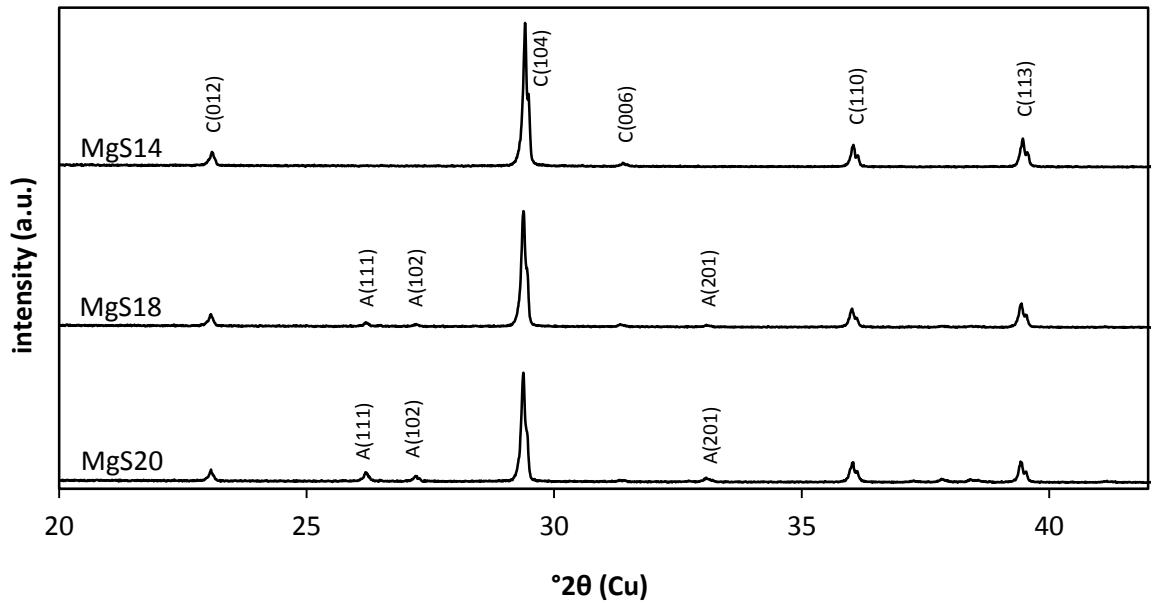

Fig. 5: XRD patterns of precipitates collected after the experimental run of the experiments MgS14, MgS18 and MgS20. The experiments were performed in the presence of 15 mM (d_{104} = 3.036 Å), 25 mM (d_{104} = 3.039 Å) and 30 mM (d_{104} = 3.040 Å) of sulfate, respectively, and were conducted at high growth rates ($r_P = 10^{-7 \pm 0.1}$ mol m^{-2} s^{-1}).

In accord with XRD, the SEM observations of the solid material show the occurrence of aragonite in the respective samples. Needle-like aragonite prisms with a pseudo hexagonal form were present in experiments MgS4, MgS5, MgS6, MgS7, MgS8, MgS16, MgS18 and MgS20 (see Fig. 8) and they were

growing mainly on the calcite seed material or were distributed randomly. The size of the aragonite crystals was increasing at elevated growth rates. In Fig. 7A it can be seen that the precipitated calcite at low growth rates kept the same rhombohedral morphology as the initial calcite seed material (see Fig. 6A) whereas the shape of precipitated calcite at elevated growth rates was scalenohedral, which is shown in Fig. 7B. Most prominent was the observed porous surface structure of calcite grown in the presence of sulfate (see Fig. 6B). The Mg content of the precipitates (in mol%) sampled at the end of the experimental run was calculated according to the equation

$$X_{Mg} = \frac{n_{Mg}}{n_{Mg}+n_{Ca}} \times 100 \quad (13)$$

where n_{Mg} and n_{Ca} are based on measurements of the solids using ICP-OES after digestion in HNO_3 and after n_{Ca} was corrected for the amount of precipitated calcite. The results are listed in Table 1. The possible amount of incorporated sulfate into the solid lattice was not quantified in this study.

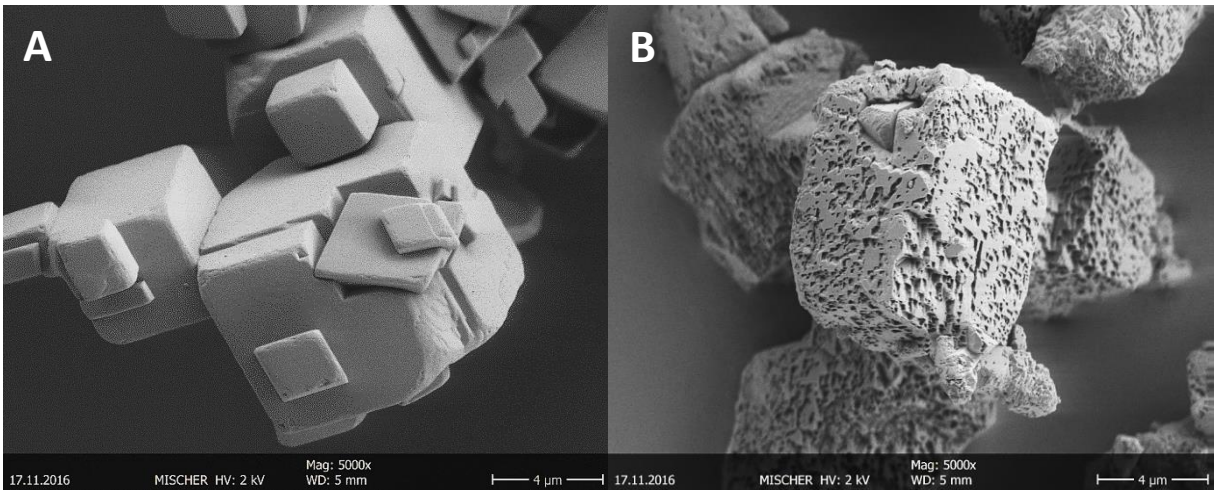

Fig. 6: SEM images of seed material before the experimental run and precipitates after the experimental run. A: Calcite seed material. B: Collected material after the experimental run of experiment MgS1 with a sulfate concentration of 30 mM in the reactive solution and conducted at low growth rate.

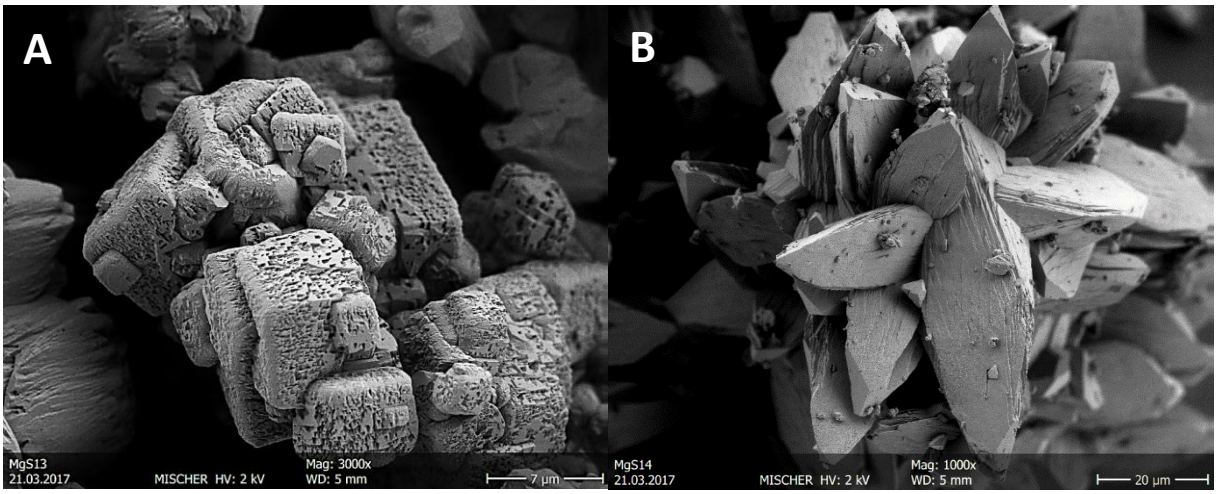

Fig. 7: SEM images of collected material after the experimental run of experiments MgS13 and MgS14, which were performed in the presence of 15 mM sulfate and conducted at different growth rates. A: (low growth rate) Calcite overgrowths with a prominent porous surface structure. B: (high growth rate) Calcite with scalenohedral crystal shape.

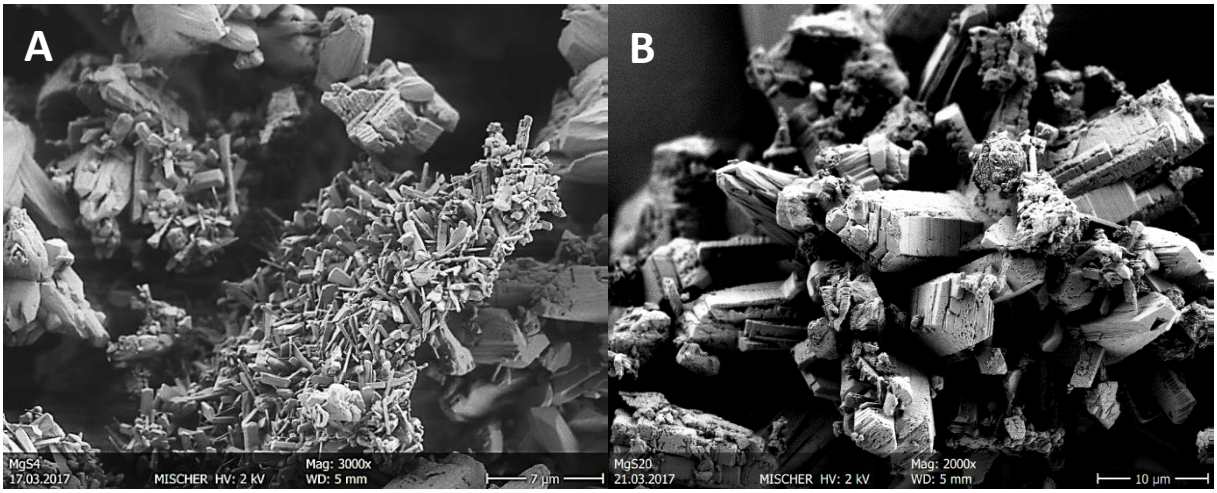

Fig. 8: SEM images of precipitates collected after the experimental run of experiments MgS4 and MgS20, which were performed in the presence of 30 mM sulfate. The precipitates consisted of a mixture of calcite and aragonite. A and B: Needle-like aragonite with pseudo-hexagonal form was observed.

4.3 Mg partitioning between calcite and fluid

The partitioning coefficient of Mg, D_{Mg}, between calcite and reactive fluid at chemical steady-state conditions has been determined from the number of moles of Ca and Mg measured in the solids collected after the experimental run and the number of moles of Ca and Mg in the reactive fluid as:

$$D_{Mg} = \frac{\left(\frac{n_{Mg}}{n_{Ca}}\right)_{calcite}}{\left(\frac{n_{Mg(ss)}}{n_{Ca(ss)}}\right)_{fluid}} \quad (14)$$

where n_{Mg} and n_{Ca} of the solid have been measured by ICP-OES after digestion in HNO_3 and have been corrected for the proportion of precipitated calcite according to the quantitative XRD results and the amount of the seed material. Calculated average values for $n_{Mg(ss)}$ and $n_{Ca(ss)}$ denote the aqueous molar concentrations of free Mg^{2+} and Ca^{2+} ions at steady-state conditions in the reactor and were estimated using PHREEQC software together with its minteq.v4 database. The results of speciation calculation indicate that the Ca^{2+} and Mg^{2+} free ions, only in the two experiments in the absence of sulfate, account for more than 94 % of total aqueous Ca and Mg present in the reactive solution, consistent with the percentage reported earlier by Mavromatis et al. (2013; 2017). In the presence of 30 mM sulfate in the reactive solution, 25 % of the total aqueous Mg and more than 30 % of the total aqueous Ca was complexed and corrections for Mg and Ca complexation were necessary in order to determine D_{Mg} values. The proportion of complexed Mg is decreasing with lower concentrations of sulfate present in the reactive solution according to the results of speciation calculation.

Results of Mg partitioning calculated for the 20 co-precipitation experiments in the presence and absence of sulfate are listed in Table 1 and are plotted as a function of growth rate in Fig. 9. As it was earlier established, D_{Mg} increases with the solution saturation state with respect to calcite and consequently with calcite precipitation rate (Mavromatis et al., 2013). D_{Mg} values obtained in this study ($0.01 \leq D_{Mg} \leq 0.04$) are in good agreement with the available experimental data at 25 °C (Oomori et al., 1987; Mucci, 1987; Howson et al., 1987; Burton and Walter, 1991; Hartley and Mucci, 1996; Huang and Fairchild, 2001). The results indicate a positive correlation between D_{Mg} and calcite growth rate (Fig. 9), where a negative correlation between D_{Mg} and sulfate concentrations in the reactive solution exists at constant calcite growth rate (Fig. 10). The red dotted line in Fig. 9 indicates the theoretical line for experiments in the absence of sulfate in the reactive solution. All experiments performed in the presence of sulfate plot below this line. D_{Mg} is significantly affected by the presence of dissolved sulfate and the subsequent formation of aqueous complexes (e.g. $CaSO_4^0$ and $MgSO_4^0$). Indeed, as it can be seen in Fig. 10, D_{Mg} values are decreasing at higher sulfate concentrations of the reactive solution and in the absence of mineral growth rate effects.

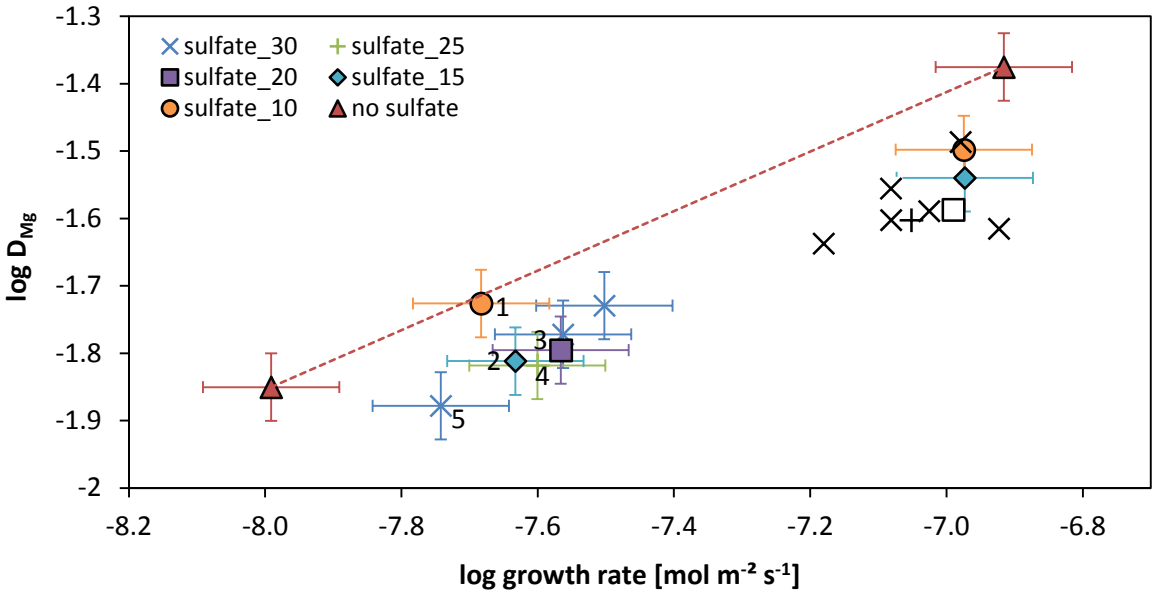

Fig. 9: Mg partitioning coefficient, D_{Mg}, between calcite and fluid plotted as a function of calcite growth rate. The red dotted line indicates the theoretical line for experiments in the absence of sulfate. The numbers in the legend denote the sulfate concentration in mM present in the reactive solution. Analytical uncertainty is given by the error bars. The black (colourless) symbols indicate precipitates which contain aragonite beside calcite (cannot be used to calculate the precise growth rate of calcite). The numbers 1-5 next to the data points are identical the same data points plotted in Fig. 10.

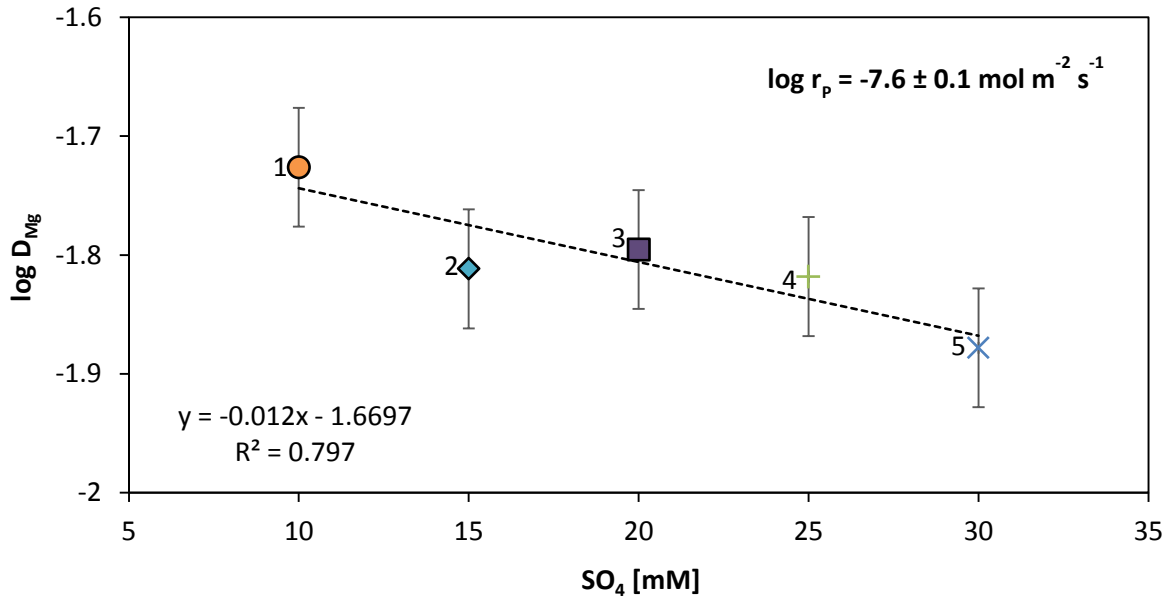

Fig. 10: D_{Mg} affected by the presence of SO_4 in the reactive solution and in absence of growth rate effects. Experiments were conducted at low growth rate ($r_P = 10^{-7.6 \pm 0.1}$ mol m^{-2} s^{-1}).

5. Interpretation and Discussion

5.1 Controls on mineralogy and surface structure

The change of the mineralogy of the precipitate from calcite to aragonite in the overgrowths of the present study, as they are presented in Table 1, suggest that mineral growth is not controlled only by the classical terrace-ledge-kink (TLK) model of crystal growth (Burton et al., 1951; Chernov, 1984), but a second mechanism takes place at the conducted experiments. Indeed the presence of seed material in overgrowth experiments generally assure that the precipitating mineral phase is that of the seed (Lin and Singer, 2005). One of the critical requirements for ongoing crystal overgrowth is the molecular level of recognition of the seed surface (Stumm and Morgan, 1996). In the experiments conducted in this study, however, aragonite grows on calcite seeds and/or nucleates from the fluid, although the supersaturation of the reactive solution in respect to calcite was higher than that in respect to aragonite (see Fig. 11). Considering that in similar experimental runs conducted earlier by Mavromatis et al. (2013; 2017), and revised herein, low Mg-calcite (< 1.7 mol% $MgCO_3$) precipitated as overgrowth on calcite seed material, there is evidence for a specific control on the formation of $CaCO_3$ polymorphs despite the presence of calcite seed material.

Experimental studies have shown that increasing Mg/Ca ratios induce a mineralogical change of precipitates from seawater at 25 °C, causing aragonite to precipitate instead of calcite at aqueous Mg/Ca ratios higher than ~ 1 (Morse et al., 1997). Note here that solely nucleation of aragonite on seed material was not observed in any of the experimental runs, however precipitates with different proportions of calcite and aragonite were observed in 8 experiments (Table 1). Actually, aragonite nucleation in the reactive solution occurred only above a certain degree of oversaturation of the reactive solution with respect to this mineral phase ($\Omega_{aragonite} > 2.9$; Fig. 11). As aragonite nucleation is a function of supersaturation, this certain limit in $\Omega_{aragonite}$ value is required to overcome the energy barrier of nucleation at the prevailing conditions (De Yoreo and Vekilov, 2003). Thus driving force for the nucleation of aragonite is its high supersaturation and thus it is present only in experiments conducted at high precipitation rates. Moreover there is evidence that calcite growth is inhibited by adsorption of SO_4^{2-} ions at calcite growth sites (Nielsen et al., 2016), in similar terms to the presence of phosphate ions. Crystallization of calcite in the presence of aqueous phosphates is retarded due to adsorption phenomena (Katsifaras and Spanos, 1999).

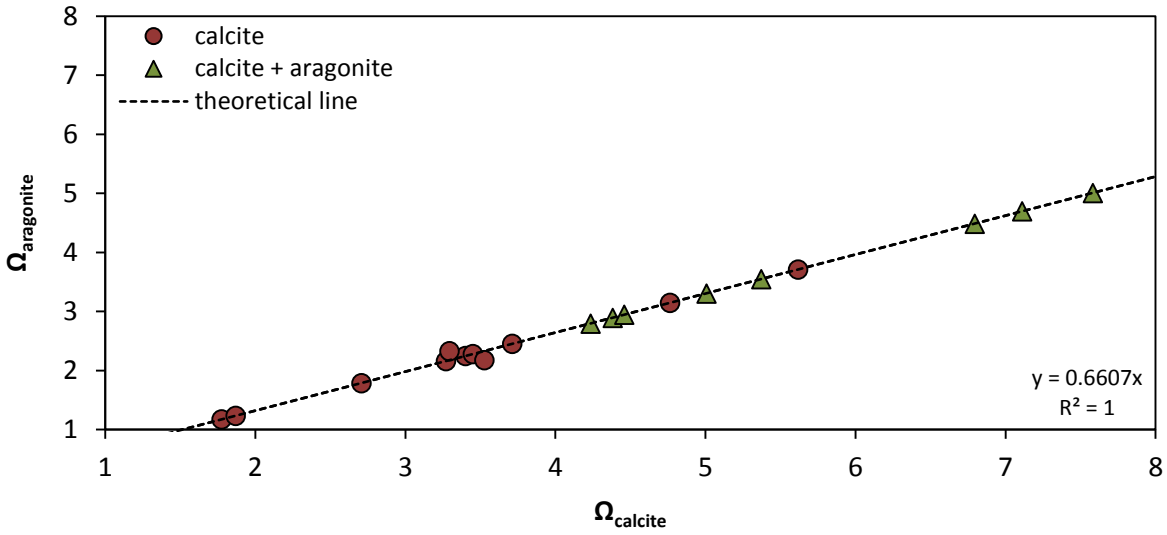

Fig. 11: Saturation degree (Ω) with respect to aragonite versus Ω with respect to calcite in all experimental runs.

Therefore, besides adsorption of Mg^{2+} ions on calcite seed crystals, the adsorption of sulfate on crystal growth sites, that is poisoning them (Gratz and Hillner, 1993), is an additional parameter which is controlling calcite surface overgrowth. In experiments MgS12 and MgS14, that were conducted at high growth rates and exhibit $\Omega_{aragonite} > 4$, aragonite is not formed. In these experiments sulfate concentration in the reactive solution was low (10 and 15 mM; see Table 1). This points towards the theory that there is a much stronger poisoning of the calcite crystallization sites at higher concentrations of sulfate (20 to 30 mM) in the reactive solution. As soon as growth positions at the crystal surface are blocked or disturbed, e.g. by adsorption of foreign ions (in this case magnesium and sulfate ions or their aquo-complexes), new molecules cannot adapt at the surface (Reddy and Wang, 1980; Meyer, 1984). This can result in an inhibited crystal overgrowth of calcite and a preferred nucleation of aragonite. Note here that the formation of aragonite instead of the thermodynamically more stable calcite in the present study cannot be solely attributed to the inhibition of the latter due to the prevailing Mg^{2+}/Ca^{2+} ratio in solution (Lippmann, 1973; Berner, 1975; Reddy and Wang, 1980). Evidence for this comes from the fact that similar aqueous Mg^{2+}/Ca^{2+} ratios at chemical steady-state are met in all the experimental runs ($0.3 \leq Mg^{2+}/Ca^{2+} \leq 0.5$). In Fig. 12 it can be seen that precipitation of aragonite occurs only after a threshold saturation value in respect to aragonite is reached and a certain concentration of sulfate is present in the reactive solution. Thus aragonite nucleation is triggered by the adsorption of both Mg and sulfate ions on the growing calcite crystals. More specifically the inhibition effect of this ions follows the order $SO_4^{2-} < Mg^{2+} < MgSO_4^0$ as it has been recently suggested by Nielsen et al. (2016) that have studied the combined effects of Mg^{2+} and SO_4^{2-} during calcite growth.

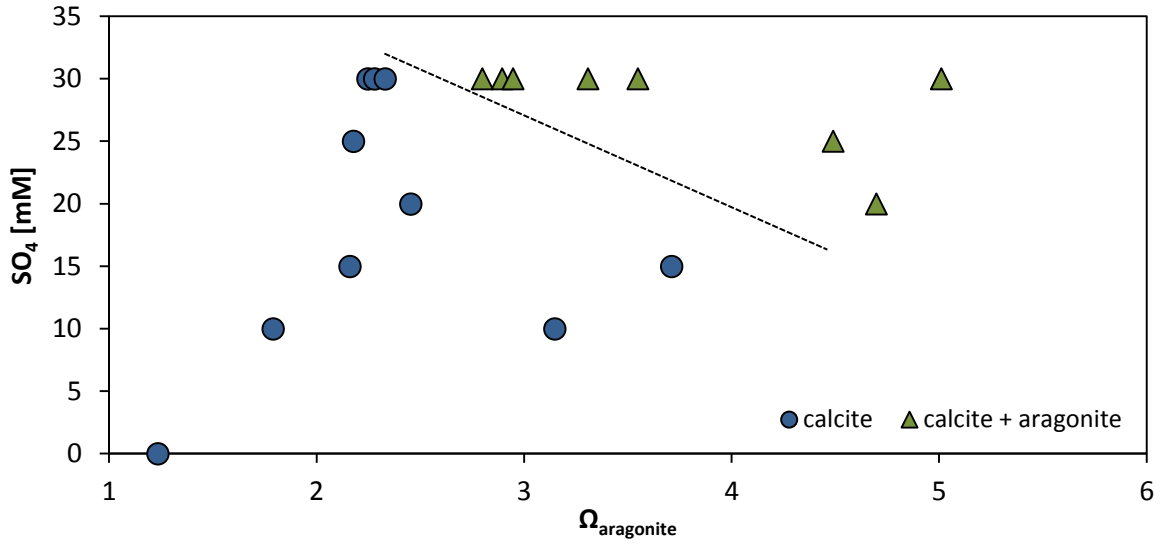

Fig. 12: Saturation state $\Omega_{aragonite}$ versus sulfate concentration in the reactive solution. Precipitation/nucleation of aragonite occurs at $\Omega_{aragonite}$ values > 2.9 in the presence of 30 mM sulfate in the reactive solution. At lower sulfate concentrations (20 and 25 mM) a higher degree of saturation state in respect to aragonite is required to nucleate aragonite beside calcite.

Adsorption and incorporation of impurities during growth can cause the calcite crystal morphology to change (Zhang and Dawe, 2000). Indeed, the SEM images of calcite recovered at the end of the experimental runs show a change in the surface structure of the overgrowths. The highly porous structure, which was observed on calcite precipitates conducted at low growth rates, suggests that adsorption of foreign molecules occurs on distinct crystal growth sites. The adsorbed molecules may disturb the growth mechanism creating a porous crystal surface (see Fig. 6B and Fig. 7A). Also the incorporation of Mg in the calcite overgrowth could be responsible for a change in the morphology due to the difference in the ionic radii of Mg and Ca that are 0.72 Å and 1.0 Å respectively. Another observation was a differing calcite crystal habitus in experiments conducted at high growth rates. At high growth rates, dog-tooth (scalenohedral) shapes of the calcite crystals were observed, whereas at low growth rates the rhombohedral form of the seed material was maintained (see Fig. 7B). Calcite is known to show astonishingly variable habitus, where a dog-tooth habitus is obtained e.g. by adding an impurity component in the precipitating solution (Sunagawa, 2005). In this study the habitus is obviously changing with growth rates and consequently higher supersaturation. There was no change observed in habitus between seed and precipitate in experiments conducted at low growth rates but with the same concentrations of impurities (Mg and SO_4) in the reactive solution.

5.2 Controls on Mg partitioning

The obtained results illustrate that the growth rate and the presence of dissolved SO_4^{2-} in the reactive solution significantly affect the partitioning coefficient of Mg in the forming calcite (see Fig. 9 and Fig. 10, respectively). It has been earlier shown that the effect of growth rate has a major control on trace element incorporation in calcium carbonate for a number of divalent cations (e.g. Lorens, 1981; Mucci and Morse, 1983; Tesoriero and Pankow, 1996; Huang and Fairchild, 2001; Tang et al., 2008; Mavromatis et al., 2013; Gabitov et al., 2014) as well as anions (e.g. Busenberg and Plummer, 1985; House and Donaldson, 1986; Mavromatis et al., 2015). Accordingly, in this study we obtained a significant increase of D_{Mg} in calcite with increasing growth rate as it is shown in Fig. 9. This is because at higher growth rates there is less discrimination in respect to elemental uptake which can be explained e.g. by the growth entrapment model (GEM) developed by Watson and Liang (1995). According to this model the incorporation of Mg into the calcite crystal structure depends on the crystal growth kinetics and the ion diffusion behaviour within a reactive surface layer in the vicinity of the growing crystal. As it is suggested by Watson (1996; 2004) the incorporation of traces into calcite is dependent on the enrichment or depletion of impurities in the distorted and hydrated thin layer present at the crystal surface. The entrapment of Mg will be favoured as soon as Mg^{2+} is enriched in the surface layer and precipitation takes place at rapid growth rates.

Beside the effect of growth rate, we observed that the presence of dissolved sulfate in the reactive solution affects the Mg partitioning of the forming calcite. The general trend is an increasing Mg partitioning in calcite with increasing growth rate, but to discriminate between growth rate and surface complexation effect it is necessary to have a closer look on the experiments in the absence of growth rate effects as it is shown in Fig. 10. In this way the limiting effects of dissolved sulfate present in the reactive solution on the Mg incorporation in calcite get visible as there is a negative correlation of D_{Mg} as a function of sulfate concentration. This finding is in good agreement with that of Mucci et al. (1989) who examined the influence of dissolved SO_4^{2-} ions on the amount of Mg^{2+} incorporated in Mg-calcite overgrowths in artificial seawater solutions at 25 °C. The Mg distribution coefficient in calcite precipitated from sulfate-free seawater was 34 % larger than precipitated from “normal” seawater.

Hydrogeochemical modelling revealed that Ca and Mg form strong aquo-complexes with SO_4 as it is listed in Table A in the Appendix. In Fig. 13 it is shown that $CaSO_4^0{}_{(aq)}$ is the stronger complex compared to $MgSO_4^0{}_{(aq)}$ in the reactive solution. This is because (i) the stability constant for $CaSO_4^0{}_{(aq)}$ ($K = 10^{2.36}$) is higher than the stability constant for $MgSO_4^0{}_{(aq)}$ ($K = 10^{2.26}$) and (ii) aqueous Ca concentration is higher compared to that of Mg in all experimental runs. The values of aqueous speciation reported in this study were calculated using PHREEQC and its minteq.v4 database which is derived from NIST46.3 database. Note here that different databases (e.g. phreeqc, llnl, etc.) provide slightly different values

for the stability constants. In consequence of aquo-complex formation with sulfate, the Mg^{2+}/Ca^{2+} ratio in the aqueous solution is changing to higher values compared to the total Mg/Ca ratio due to the preferential formation of $CaSO_4^0{}_{(aq)}$ complexes (see Fig. 14).

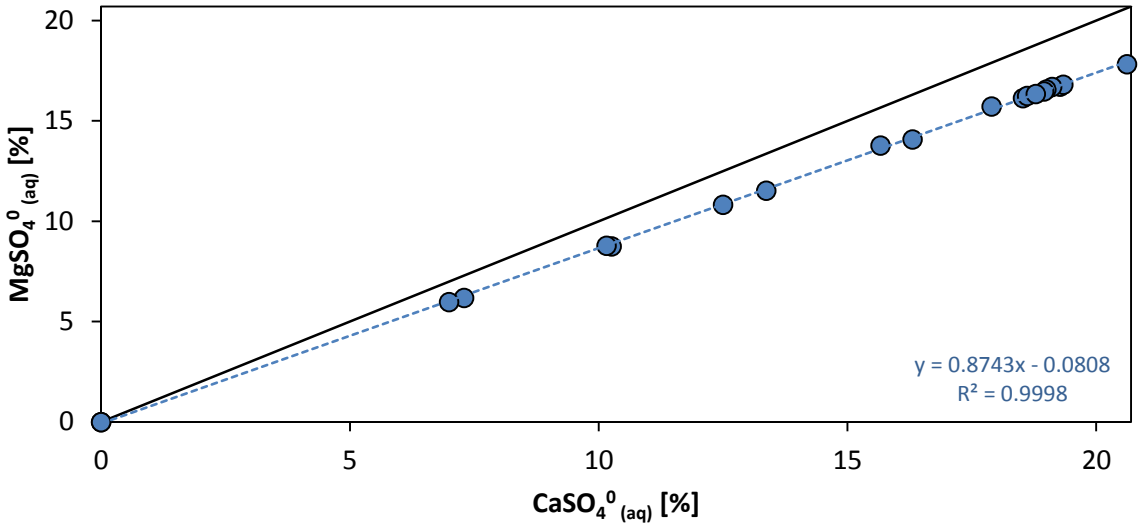

Fig. 13: $MgSO_4^0{}_{(aq)}$ complexation versus $CaSO_4^0{}_{(aq)}$ complexation. The solid line indicates the 1:1 ratio.

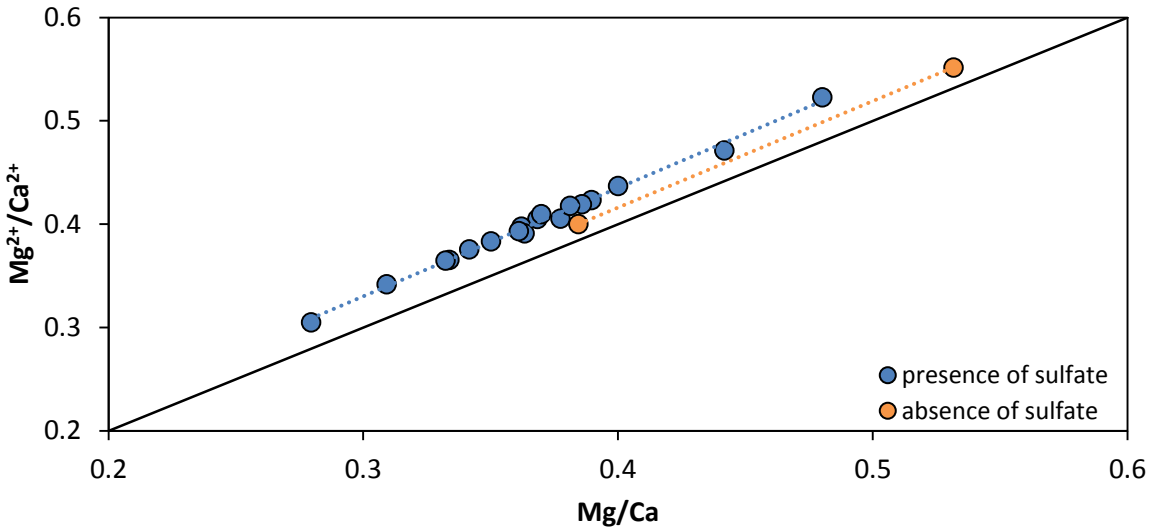

Fig. 14: Active Mg^{2+}/Ca^{2+} ratio plotted against total aqueous Mg/Ca ratio in the reactive solution at chemical steady state. The solid line indicates the 1:1 ratio. In the presence of sulfate the active Mg^{2+}/Ca^{2+} ratio in the aqueous solution is changing to higher values.

Due to the higher Mg^{2+}/Ca^{2+} ratios compared to the total Mg/Ca ratios, increasing values of D_{Mg} as a function of sulfate concentration are expected, but within this study, the opposite was observed. As the Mg^{2+}/Ca^{2+} ratio cannot be considered in this case as a parameter explaining the decreasing Mg incorporation in calcite with increasing sulfate concentrations in the reactive solution, a different mechanism has to be the trigger. Thus the lower D_{Mg} values of calcite in the absence of growth rate effects (Fig. 10) are likely caused by processes occurring at or near the surface of the growing crystal.

As it has been shown earlier the partitioning of a cation like Mg, that is relatively incompatible in the calcite lattice ($D_{Me} < 1$) is favoured at rapid growth rates (Mavromatis et al., 2013). But the adsorption of sulfate ions or sulfate-bearing complexes on the surface may disturb the Mg uptake. Molecular dynamic simulations of $CaCO_3$ and $MgCO_3$ growth at calcite surface show that Mg^{2+} can be easily incorporated into growth steps (De Leeuw, 2002) and it is known from experimental studies that subsequently incorporation of Mg^{2+} strongly inhibits further calcite growth (Berner, 1975; Meyer, 1984). Ahsan and Fabricius (2010) claimed that Mg^{2+} is competing SO_4^{2-} ions in adsorption behavior at the calcite surface. Mg^{2+} is found to be preferentially adsorbed at the acute steps of the calcite surface (Davis et al., 2004). At the upper edge of acute steps also CO_3^{2-} adsorption preferentially occurs (De La Pierre et al., 2017), while further Me^{2+} ions only adsorbs at this step after CO_3^{2-} adsorption. A similar kind of competition in surface-complex formation on the calcite surface might be also causing the decreased Mg incorporation during calcite growth in the present of sulfate, found in this study. To determine the inverse Mg^{2+} and SO_4^{2-} incorporation behavior in calcite, further studies are required to validate this approach.

The presence of sulfate in the reactive solution has a significant impact on the Ca and Mg species distribution, as > 30 % of the total Ca and > 24 % of the total Mg are complexed in the presence of 30 mM sulfate, whereas in the absence of sulfate Ca and Mg are complexed < 10 % and < 6 % respectively. This is an important finding as species distribution in the reactive solution is controlling not only the surface complexation and the Mg partitioning in calcite, but also the growth kinetics and the resulting polymorph. The inhibition effects of sulfate on crystal growth and Mg incorporation follows two mechanisms that operate simultaneously. The first is the calcite growth inhibition due to the complexation of Ca^{2+} with SO_4^{2-} ions that lowers the total availability of Ca^{2+} free ions. The second is the adsorption of foreign molecules on the Mg-active surface sites, e.g. negative steps, which causes poisoning or blocking of these crystal growth sites. This means, the more complexes in the fluid, the more growth sites can be blocked. Both mechanisms are resulting to lower D_{Mg} values in calcite which is controlled by the sulfate concentration present in the reactive solution.

5.3 Implications for natural systems

Sulfate is the second most concentrated anion in seawater and it forms strong complexes with Ca^{2+} and Mg^{2+} in aqueous solutions. Up to now only a few studies investigate the role of dissolved SO_4^{2-} on the formation of calcium carbonate minerals (Takano, 1985; Mucci et al., 1989; Fernández-Díaz et al., 2010; Bots et al., 2011; Flaathen et al., 2011; Nielsen et al., 2016; Han et al., 2017). Bots et al. (2011) correlated the primary inorganic calcium carbonate mineralogy, which was oscillating between calcite and aragonite throughout the Phanerozoic, to changes in the seawater chemistry. They suggest that 1.5 mol% SO_4 incorporation into the carbonate minerals had a little effect on the aragonite structure (increase of c-axis and b-axis by ~0.07 % and ~0.02 % respectively) compared to calcite (increase of c-axis by ~0.22 % and decrease of a-axis by ~0.035 %). The calcite solubility increases from $10^{-8.48}$ to $10^{-8.33}$ due to the change in the calcite structure by incorporation of > 4 mol% SO_4 so that calcite becomes more soluble than pure aragonite (Busenberg and Plummer, 1985). This demonstrates that SO_4 increases the stability of aragonite vs. calcite, which may explain the precipitation of aragonite instead of calcite at Mg/Ca ratios < 0.9 in the presence of sulfate. In any case, the results of the calculations by Fernández-Díaz et al. (2010), who examined the role of sulfate groups in controlling $CaCO_3$ polymorphism, showed that the substitution of sulfate for carbonate groups into aragonite is less favorable than into calcite.

From the experiments in this study at low growth rate (log r_P = 7.6 ± 0.1 mol m^{-2} s^{-1}) we can assume that the total incorporation of impurities, both Mg and SO_4, is controlled by both growth rate and surface complexation. We do not see precipitation of aragonite at low growth rate, although the concentration of sulfate was the same as in experiments conducted at high growth rate. In the latter case the highest proportions of aragonite were observed. Thus it is suggested that the adsorption of SO_4^{2-} on calcite surface combined with high growth rates controls the forming polymorph. It is worth noting here that adsorption is a reversible reaction and dynamic equilibrium between dissolved and sorbed species which assures that no calcite surface site is permanently blocked. Yet at high growth rates, adsorbed sulfate ions may get overgrown by the newly forming crystal layers, causing disorder phenomena in the crystal lattice.

The results of this study indicate that the presence of sulfate and its complexation with divalent cations can significantly decrease the Mg uptake during calcite precipitation in the absence of an overall growth rate effect. This may play an important role in our understanding of the parameters controlling biomineralisation processes as well as abiotically formed calcium carbonates and implies a demand for re-examining the validity of D_{Mg} for the reconstruction of the physicochemical conditions during calcite growth in natural settings e.g. growth rate, temperature. Indeed, the application of the results of the present work to sedimentary environments is straightforward because precipitation rates performed

in this study overlap most calcite precipitation rates measured in various environments and the used concentration of SO_4 (30 mM) in the reactive solution represents the prevailing concentration of sulfate in seawater which is about 2700 ppm. As soon as sediment is setteld on the seafloor and early burial is ongoing, the anaerobic oxidation of methane (AOM) and bacterial sulfate reduction takes place. With ongoing sulfate reduction, alkalinity is increasing in the pore solutions and precipitation of carbonate minerals takes place. The concentration of sulfate is usually decreasing with increasing depth as it can be seen in Fig. 15, due to the fact that SO_4^{2-} is the oxygen source that is used immediately after the consumption of dissolved O_2. Therefore the experiments conducted at lower sulfate concentrations (25 mM, 20 mM, 15 mM and 10 mM) provide insights on the effect of sulfate on changes in mineralogy and Mg partitioning in calcite. This effect is reduced as there is a weaker generation of sulfate-bearing complexes and consequently the poisoning of crystal growth sites by sulfate becomes less important.

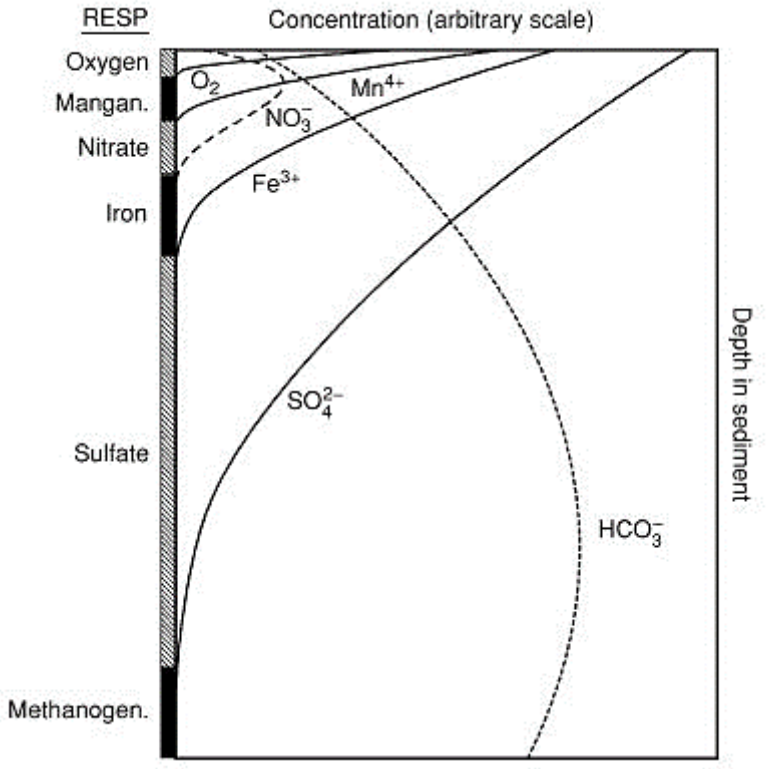

Fig. 15: Idealized vertical distribution of electron acceptors in marine sediments. The bar at the left-hand side indicates the vertical distribution of respiration pathways (Canfield et al., 2005).

6. Conclusions

The experiments performed in this study indicate that the presence of dissolved sulfate during precipitation of $CaCO_3$ controls the polymorph formation even if mono-mineralogical seeds (in this case calcite) are present. Moreover aqueous sulfate may affect the surface morphology of the overgrowth as well as the incorporation behaviour of Mg during calcite formation. Mineral growth rate is another highly important parameter evaluated in this study. The outcome of the experiments documented here show a main dependence of Mg incorporation in calcite on the control of the growth rate. The combined impact of the composition of the solution chemisty and the varying growth rate results in precipitates with variable mineralogical and chemical compositions.

In the presence of 30 mM of sulfate in the reactive solution the composition of the precipitate was based on calcite or a mixture of calcite and aragonite, whereas the precipitation of aragonite was observed in experiments conducted at high growth rates and sulfate concentrations ranging from 20 to 30 mM. At lower concentrations of dissolved sulfate (15 mM, 10 mM) in the reactive solution, calcite was the only forming solid phase even in experiments conducted at high growth rates. Sulfate is forming strong $CaSO_4^0{}_{(aq)}$ and $MgSO_4^0{}_{(aq)}$ complexes in aqueous solutions. The control of dissolved SO_4^{2-} and its aquo-complex formation on the mineralogy can be explained by the adsorption of sulfate-bearing complexes on the crystal surface during mineral growth, which is resulting in poisoning of calcite crystal growth sites. This results in an inhibition of crystal overgrowth of calcite and a preferred nucleation of aragonite but also an inhibited incorporation of Mg during calcite growth.

The Mg partitioning between calcite and the reactive solution increases at higher calcite growth rate. In the absence of growth rate effects, increasing concentrations of dissolved sulfate in the reactive solution, result in significantly decreasing incorporation of Mg in calcite. The effect of sulfate on Mg partitioning can be described by two mechanisms: (i) the inhibition of calcite growth by aquo-complex formation between Ca^{2+} and SO_4^{2-} and (ii) the blocking of Mg-active growth steps by adsorption of sulfate molecules. It is likely that SO_4^{2-} ions or sulfate-bearing complexes adsorb on the acute steps and consequently block the growth sites for Mg incorporation in calcite. Accordingly, adsorption of sulfate on crystal growth sites, can result in lower D_{Mg} values for calcite, likely due to competition of adsorption of Mg^{2+} and sulfate-bearing complexes on similar surface growth sites.

The incorporation of foreign cations or impurities into carbonate minerals is mostly controlled by the chemical composition of the solution, growth rate, and temperature. Thus, analysis of the chemical and isotopic composition of carbonates is likely to be a very useful tool to unravel environmental conditions during carbonate mineral formation. Laboratory experiments will be essential to provide insights about the controls of environmental changes on the formation of calcium carbonate minerals.

References

Ahsan R. and Fabricius I. L. (2010) Sorption of Magnesium and Sulfate Ions on Calcite. In *72nd EAGE Conference*

Appelo C. A. J. and Postma D. (2005) *Geochemistry, groundwater and pollution*. 2nd ed., A.A. Balkema Publishers, Amsterdam, the Netherlands.

Berner R. A. (1975) The role of magnesium in the crystal growth of calcite and aragonite from sea water. *Geochim. Cosmochim. Acta* **39**, 489–504.

Bots P., Benning L. G., Rickaby R. E. M. and Shaw S. (2011) The role of SO_4 in the switch from calcite to aragonite seas. *Geology* **39**, 331–334.

Böttcher M. E. and Dietzel M. (2010) Metal-ion partitioning during low-temperature precipitation and dissolution of anhydrous carbonates and sulphates. *EMU notes Mineral.* **10**, 139–187.

Braissant O., Decho A. W., Dupraz C., Glunk C., Przekop K. M. and Visscher P. T. (2007) Exopolymeric substances of sulfate-reducing bacteria: Interactions with calcium at alkaline pH and implication for formation of carbonate minerals. *Geobiology* **5**, 401–411.

Burton E. A. and Walter L. M. (1991) The effects of pCO_2 and temperature on magnesium incorporation in calcite in seawater and $MgCl_2$-$CaCl_2$ solutions. *Geochim. Cosmochim. Acta* **55**, 777–785.

Burton W. K., Cabrera N. and Frank F. C. (1951) The Growth of Crystals and the Equilibrium Structure of their Surfaces. *Phil. Trans. R. Soc. Lond.* **243**, 299–358.

Busenberg E. and Plummer L. N. (1985) Kinetic and thermodynamic factors controlling the distribution of SO_4^{2-} and Na^+ in calcites and selected aragonites. *Geochim. Cosmochim. Acta* **49**, 713–725.

Busenberg E. and Plummer N. L. (1989) Thermodynamics of magnesian calcite solid-solutions at 25 °C and 1 atm total pressure. *Geochim. Cosmochim. Acta* **53**, 1189–1208.

Canfield D. E., Kristensen E. and Thamdrup B. (2005) Heterotrophic Carbon Metabolism. *Adv. Mar. Biol.* **48**, 129–162.

Chernov A. A. (1984) *Modern Crystallography III*., Springer-Verlag.

Davis K. J., Dove P. M., Wasylenki L. E. and De Yoreo J. J. (2004) Morphological consequences of differential Mg^{2+} incorporation at structurally distinct steps on calcite. *Am. Mineral.* **89**, 714–720.

Dietzel M. (2011) Carbonates. *Encycl. Geobiol.*, 261–266.

Dupraz C., Visscher P. T., Baumgartner L. K. and Reid R. P. (2004) Microbe-mineral interactions: Early carbonate precipitation in a hypersaline lake (Eleuthera Island, Bahamas). *Sedimentology* **51**, 745–765.

Fernández-Díaz L., Fernández-González Á. and Prieto M. (2010) The role of sulfate groups in controlling $CaCO_3$ polymorphism. *Geochim. Cosmochim. Acta* **74**, 6064–6076.

Flaathen T. K., Oelkers E. H., Gislason S. R. and Aagaard P. (2011) The effect of dissolved sulphate on calcite precipitation kinetics and consequences for subsurface CO_2 storage. *Energy Procedia* **4**, 5037–5043.

Gabitov R. I., Sadekov A. and Leinweber A. (2014) Crystal growth rate effect on Mg/Ca and Sr/Ca partitioning between calcite and fluid: An in situ approach. *Chem. Geol.* **367**, 70–82.

Gaetani G. A. and Cohen A. L. (2006) Element partitioning during precipitation of aragonite from seawater: A framework for understanding paleoproxies. *Geochim. Cosmochim. Acta* **70**, 4617–4634.

Glynn P. (2000) Solid-Solution Solubilities and Thermodynamics: Sulfates, Carbonates and Halides. *Rev. Mineral. Geochemistry* **40**, 481–511.

Goldsmith J. R., Graf D. L. and Heard H. C. (1961) Lattice constants of the calcium-magnesium carbonates. *Am. Mineral.* **46**, 453–459.

Gratz A. J. and Hillner P. E. (1993) Poisoning of calcite growth viewed in the atomic force microscope (AFM). *J. Cryst. Growth* **129**, 789–793.

Han M., Zhao Y., Zhao H., Han Z., Yan H., Sun B., Meng R., Zhuang D., Li D. and Liu B. (2017) A comparison of amorphous calcium carbonate crystallization in aqueous solutions of $MgCl_2$ and $MgSO_4$: implications for paleo-ocean chemistry. *Mineral. Petrol.* **0**, 1–16.

Hartley G. and Mucci A. (1996) The influence of pCO_2 on the partitioning of magnesium in calcite overgrowths precipitated from artificial seawater at 25 ° and 1 atm total pressure. *Geochim. Cosmochim. Acta* **60**, 315–324.

House W. A. and Donaldson L. (1986) Adsorption and coprecipitation of phosphate on calcite. *J. Colloid Interface Sci.* **112**, 309–324.

Hover V. C., Walter L. M. and Peacor D. R. (2001) Early marine diagenesis of biogenic aragonite and Mg-calcite: New constraints from high-resolution STEM and AEM analyses of modern platform carbonates. *Chem. Geol.* **175**, 221–248.

Howson M. R., Pethybridge A. D. and House W. A. (1987) Synthesis and distribution coefficient of low-magnesium calcites. *Chem. Geol.* **64**, 79–87.

Huang Y. and Fairchild I. J. (2001) Partitioning of Sr^{2+} and Mg^{2+} into calcite under karst-analogue experimental conditions. *Geochim. Cosmochim. Acta* **65**, 47–62.

Katsifaras A. and Spanos N. (1999) Effect of inorganic phosphate ions on the spontaneous precipitation of vaterite and on the transformation of vaterite to calcite. *J. Cryst. Growth* **204**, 183–190.

Kitano Y., Okumura M. and Idogaki M. (1975) Incorporation of sodium, chloride and sulfate with calcium carbonate. *Geochem. J.* **9**, 75–84.

Koutsoukos P. G. and Kontoyannis C. G. (1984) Precipitation of calcium carbonate in aqueous solutions. *Faraday Trans.* **80**, 1181–1192.

De La Pierre M., Raiteri P., Stack A. G. and Gale J. D. (2017) Uncovering the Atomistic Mechanism for Calcite Step Growth. *Angew. Chemie - Int. Ed.* **56**, 8464–8467.

De Leeuw N. H. (2002) Surface structures, stabilities, and growth of magnesian calcites: A computational investigation from the perspective of dolomite formation. *Am. Mineral.* **87**, 679–689.

Lin Y. P. and Singer P. C. (2009) Effect of Mg^{2+} on the kinetics of calcite crystal growth. *J. Cryst. Growth* **312**, 136–140.

Lin Y. P. and Singer P. C. (2005) Effects of seed material and solution composition on calcite precipitation. *Geochim. Cosmochim. Acta* **69**, 4495–4504.

Lippmann F. (1973) *Sedimentary Carbonate Minerals*., Springer, Berlin.

Lorens R. B. (1981) Sr, Cd, Mn and Co distribution coefficients in calcite as a function of calcite precipitation rate. *Geochim. Cosmochim. Acta* **45**, 553–561.

Marriott C. S., Henderson G. M., Crompton R., Staubwasser M. and Shaw S. (2004) Effect of mineralogy, salinity, and temperature on Li/Ca and Li isotope composition of calcium carbonate. *Chem. Geol.* **212**, 5–15.

Mavromatis V., Gautier Q., Bosc O. and Schott J. (2013) Kinetics of Mg partition and Mg stable isotope fractionation during its incorporation in calcite. *Geochim. Cosmochim. Acta* **114**, 188–203.

Mavromatis V., Immenhauser A., Buhl D., Purgstaller B., Baldermann A. and Dietzel M. (2017) Effect of organic ligands on Mg partitioning and Mg isotope fractionation during low-temperature precipitation of calcite in the absence of growth rate effects. *Geochim. Cosmochim. Acta* **207**, 139–153.

Mavromatis V., Montouillout V., Noireaux J., Gaillardet J. and Schott J. (2015) Characterization of boron incorporation and speciation in calcite and aragonite from co-precipitation experiments under controlled pH, temperature and precipitation rate. *Geochim. Cosmochim. Acta* **150**, 299–313.

Mavromatis V., Schmidt M., Botz R., Comas-Bru L. and Oelkers E. H. (2012) Experimental quantification of the effect of Mg on calcite-aqueous fluid oxygen isotope fractionation. *Chem. Geol.* **310**–**311**, 97–105.

McIntire W. L. (1963) Trace element partition coefficients - a review of theory and applications to geology. *Geochim. Cosmochim. Acta* **27**, 1209–1264.

Meyer H. J. (1984) The influence of impurities on the growth rate of calcite. *J. Cryst. Growth* **66**, 639–646.

Morse J. W., Arvidson R. S. and Lüttge A. (2007) Calcium carbonate formation and dissolution. *Chem. Rev.* **107**, 342–381.

Morse J. W. and Mackenzie F. T. (1990) *Geochemistry of sedimentary carbonates*., Elsevier, Amsterdam, Oxford, New York, Tokyo.

Morse J. W., Wang Q. and Tsio M. Y. (1997) Influences of temperature and Mg : Ca ratio on $CaCO_3$ precipitates from seawater. *Geology* **25**, 85–87.

Mucci A. (1987) Influence of temperature on the composition of magnesian calcite overgrowths precipitated from seawater. *Geochim. Cosmochim. Acta* **51**, 1977–1984.

Mucci A., Canuel R. and Zhong S. (1989) The solubility of calcite and aragonite in sulfate-free seawater and the seeded growth kinetics and composition of the precipitates at 25 °C. *Chem. Geol.* **74**, 309–320.

Mucci A. and Morse J. W. (1983) The incorporation of Mg^{2+} and Sr^{2+} into calcite overgrowths: influences of growth rate and solution composition. *Geochim. Cosmochim. Acta* **47**, 217–233.

Mucci A. and Morse J. W. (1984) The solubility of calcite in seawater of various magnesium concentrations, I_t = 0.697 m at 25 °C and one atmosphere total pressure. *Geochim. Cosmochim. Acta* **48**, 815–822.

Niedermayr A., Köhler S. J. and Dietzel M. (2013) Impacts of aqueous carbonate accumulation rate, magnesium and polyaspartic acid on calcium carbonate formation (6-40 °C). *Chem. Geol.* **340**, 105–120.

Nielsen M. R., Sand K. K., Rodriguez-Blanco J. D., Bovet N., Generosi J., Dalby K. N. and Stipp S. L. S. (2016) Inhibition of Calcite Growth: Combined Effects of Mg^{2+} and SO_4^{2-}. *Cryst. Growth Des.* **16**, 6199–6207.

Okrusch M. and Matthes S. (2014) *Mineralogie - Eine Einführung in die spezielle Mineralogie, Petrologie und Lagerstättenkunde*., Springer Spektrum, Berlin Heidelberg.

Oomori T., Kaneshima H., Maezato Y. and Kitano Y. (1987) Distribution coefficient of Mg^{2+} ions between calcite and solution at 10-50 °C. *Mar. Chem.* **20**, 327–336.

Plummer L. N. and Busenberg E. (1982) The solubilities of calcite, aragonite and vaterite in CO_2-H_2O solutions between 0 and 90 °C, and an evaluation of the aqueous model for the system $CaCO_3$-CO_2-H_2O. *Geochim. Cosmochim. Acta* **46**, 1011–1040.

Prieto M. (2010) Thermodynamics of ion partitioning in solid solution-aqueous solution systems. *EMU notes Mineral.* **10**, 1–42.

Putnis A. (2010) Effect of kinetics and mechanisms of crystal growth on ion-partitioning in solid solution-aqueous solution (SS-AS) systems. *EMU notes Mineral.* **10**, 43–64.

Reddy M. M. and Nancollas G. H. (1976) The crystallization of calcium carbonate. IV. The effect of magnesium, strontium and sulfate ions. *J. Cryst. Growth* **35**, 33–38.

Reddy M. M. and Wang K. K. (1980) Crystallization of calcium carbonate in the presence of metal ions. *J. Cryst. Growth* **50**, 470–480.

Reeburgh W. (2007) Oceanic methane biogeochemistry. *Am. Chem. Soc.* **107**, 486–513.

Rodriguez-Navarro C., Rodriguez-Gallego M., Chekroun K. Ben and Gonzalez-Muñoz M. T. (2003) Conservation of ornamental stone by Myxococcus xanthus - Induced carbonate biomineralization. *Appiled Environ. Microbiol.* **69**, 2182–2193.

Schlager W. (2005) *Carbonate Sedimentology and Sequence Stratigraphy*. 8th ed., SEPM (Society for Sedimentary Geology).

Stumm W. and Morgan J. J. (1996) *Aquatic chemistry*. 3th editio., Wiley-Interscience Publication, New York, Chichester, Brisbane, Toronto, Singapore.

Sunagawa I. (2005) *Crystals: Growth, Morphology and Perfection*., Cambridge University Press.

Takano B. (1985) Geochemical implications of sulfate in sedimentary carbonates. *Chem. Geol.* **49**, 393–403.

Tang J., Köhler S. J. and Dietzel M. (2008) Sr^{2+}/Ca^{2+} and $^{44}Ca/^{40}Ca$ fractionation during inorganic calcite formation: I. Sr incorporation. *Geochim. Cosmochim. Acta* **72**, 3718–3732.

Terakado Y. and Taniguchi M. (2006) A new method for the study of trace element partitioning between calcium carbonate and aqueous solution: A test case for Sr and Ba incorporation into calcite. *Geochem. J.* **40**, 161–170.

Tesoriero A. J. and Pankow J. F. (1996) Solid solution partitioning of Sr^{2+}, Ba^{2+}, and Cd^{2+} to calcite. *Geochim. Cosmochim. Acta* **60**, 1053–1063.

Tucker M. E. and Wright V. P. (1990) *Carbonate Sedimentology*., Blackwell Science Ltd.

Voigt M., Mavromatis V. and Oelkers E. H. (2017) The experimental determination of REE partition coefficients in the water-calcite system. *Chem. Geol.* **462**, 30–43.

Watson E. B. (2004) A conceptual model for near-surface kinetic controls on the trace- element and stable isotope composition of abiogenic calcite crystals. *Geochim. Cosmochim. Acta* **68**, 1473–1488.

Watson E. B. (1996) Surface enrichment and trace-element uptake during crystal growth. *Geochim. Cosmochim. Acta* **60**, 5013–5020.

Watson E. B. and Liang Y. (1995) A simple model for sector zoning in slowly grown crystals: implications for growth rate and lattice diffusion, with emphasis on accessory minerals in crustal rocks. *Am. Mineral.* **80**, 1179–1187.

Weiner S. and Dove P. M. (2003) An Overview of Biomineralization Processes and the Problem of the Vital Effect. *Rev. Mineral. Geochemistry* **54**, 1–29.

Xiao J., Wang Z., Tang Y. and Yang S. (2010) Biomimetic mineralization of $CaCO_3$ on a phospholipid monolayer: From an amorphous calcium carbonate precursor to calcite via vaterite. *Langmuir* **26**, 4977–4983.

De Yoreo J. J. and Vekilov P. G. (2003) Principles of Crystal Nucleation and Growth. *Rev. Mineral. Geochemistry* **54**, 57–93.

Zhang Y. and Dawe R. A. (2000) Influence of Mg^{2+} on the kinetics of calcite precipitation and calcite crystal morphology. *Chem. Geol.* **163**, 129–138.

Appendix

Table A: Distribution of aqueous Ca and Mg species, calculated using PHREEQC with its minteq.v4 database.

Experiment	**Ca TOTAL**	Ca^{+2}	$CaCO_3^0$	$CaHCO_3^+$	$CaOH^+$	$CaSO_4^0$	**Mg TOTAL**	Mg^{+2}	$MgCO_3^0$	$MgHCO_3^+$	$MgOH^+$	$MgSO_4^0$
	(× 10^{-3} M)	(× 10^{-3} M)	(× 10^{-3} M)	(× 10^{-3} M)	(× 10^{-3} M)	(× 10^{-3} M)	(× 10^{-3} M)	(× 10^{-3} M)	(× 10^{-3} M)	(× 10^{-3} M)	(× 10^{-3} M)	(× 10^{-3} M)
MgS1	15.38	10.73	9.3E-03	1.47	1.9E-06	3.17	7.39	5.61	2.6E-03	0.46	2.0E-05	1.32
MgS2	23.87	16.62	1.8E-02	2.63	3.2E-06	4.60	9.55	7.26	4.1E-03	0.69	2.7E-05	1.60
MgS3	23.76	16.42	1.8E-02	2.73	3.1E-06	4.59	7.93	6.00	3.5E-03	0.59	2.2E-05	1.33
MgS4	23.39	15.95	2.3E-02	2.95	3.5E-06	4.47	8.62	6.46	4.9E-03	0.71	2.8E-05	1.44
MgS5	24.78	16.99	2.2E-02	3.06	3.5E-06	4.71	8.97	6.75	4.6E-03	0.73	2.7E-05	1.49
MgS6	29.07	20.04	2.6E-02	3.62	4.2E-06	5.38	9.66	7.31	5.0E-03	0.79	3.0E-05	1.56
MgS7	27.68	18.96	2.8E-02	3.54	4.3E-06	5.15	9.45	7.12	5.6E-03	0.79	3.2E-05	1.54
MgS8	26.24	18.17	2.3E-02	3.08	3.9E-06	4.97	9.19	6.97	4.7E-03	0.70	3.0E-05	1.51
MgS9	18.73	17.05	7.2E-03	1.68	2.1E-06	-	9.96	9.40	2.1E-03	0.55	2.2E-05	-
MgS10	22.82	20.62	9.8E-03	2.19	2.6E-06	-	8.77	8.25	2.1E-03	0.52	2.1E-05	-
MgS11	22.02	17.82	1.4E-02	2.58	2.8E-06	1.61	9.73	8.40	3.5E-03	0.72	2.6E-05	0.60
MgS12	25.74	20.31	2.5E-02	3.61	4.0E-06	1.80	9.35	7.94	5.1E-03	0.84	3.1E-05	0.56
MgS13	26.84	20.88	1.7E-02	3.19	3.2E-06	2.75	10.13	8.47	3.7E-03	0.77	2.6E-05	0.89
MgS14	24.80	18.55	2.9E-02	3.70	4.2E-06	2.52	8.95	7.29	6.1E-03	0.87	3.3E-05	0.79
MgS15	24.54	18.09	1.9E-02	3.15	3.2E-06	3.28	9.56	7.66	4.3E-03	0.80	2.6E-05	1.10
MgS16	34.58	25.30	3.7E-02	4.92	5.5E-06	4.32	9.66	7.71	6.0E-03	0.90	3.3E-05	1.05
MgS17	25.56	18.45	1.7E-02	2.93	3.1E-06	4.17	9.86	7.74	3.8E-03	0.73	2.6E-05	1.39
MgS18	25.55	17.43	3.6E-02	4.08	4.3E-06	4.00	9.45	7.14	7.7E-03	1.00	3.5E-05	1.30
MgS19	26.66	18.43	1.9E-02	3.21	3.0E-06	5.01	10.16	7.70	4.1E-03	0.80	2.5E-05	1.66
MgS20	32.05	21.61	4.0E-02	4.67	5.3E-06	5.73	9.91	7.39	7.1E-03	0.95	3.5E-05	1.56